

REPORT DOCUMENTATION PAGE			Form Approved OMB No. 0704-0188
Public reporting burden for this collection of information is estimated to average 1 hour per response, including the time for reviewing instructions, searching existing data sources, gathering and maintaining the data needed, and completing and reviewing the collection of information. Send comments regarding this burden estimate or any other aspect of this collection of information, including suggestions for reducing this burden, to Washington Headquarters Services, Directorate for Information Operations and Reports, 1215 Jefferson Davis Highway, Suite 1204, Arlington, VA 22202-4302, and to the Office of Management and Budget, Paperwork Reduction Project (0704-0188) Washington, DC 20503.			
1. AGENCY USE ONLY (Leave Blank)	2. REPORT DATE 30 March 1998	3. REPORT TYPE AND DATES COVERED Final (01 Feb 95 – 31 Jan 98)	
4. TITLE AND SUBTITLE Pulse Propagation in Random Media			5. FUNDING NUMBERS F49620-95-1-0137
6. AUTHORS Werner E. Kohler			
7. PERFORMING ORGANIZATION NAME(S) AND ADDRESS(ES) Virginia Polytechnic and State University, Dept. of Mathematics 460 McBryde Hall Blacksburg, VA 24061-0123			AFRL-SR-BL-TR-98- 0332
9. SPONSORING/MONITORING AGENCY NAME(S) AND ADDRESS(ES) AFOSR/NM 110 Duncan Avenue, Room B-115 Bolling Air Force Base, DC 20332-8080			10. SPONSORING/MONITORING AGENCY REPORT NUMBER
11. SUPPLEMENTARY NOTES			
12a. DISTRIBUTION AVAILABILITY STATEMENT Approved for Public Release			12b. DISTRIBUTION CODE
13. ABSTRACT (Maximum 200 words)			
<p>(1) Multiple scattering of electromagnetic waves in randomly layered dissipative media. The magnetotelluric (MT) problem considered has lent itself to modeling within the "weak noise" or Gauss Markov regime. In addition to considering propagation per se, the issue of the detection of anomalous layers has been addressed. Details are presented in the enclosed preprint, "Random Scattering in Magnetotellurics," by Benjamin White, Werner Kohler, and Leonard Srnka, which has been submitted for publication to Geophysics.</p> <p>(2) Extension of the ideas mentioned above to the case of an undulating (locally layered) medium. The theory developed for layered media is shown to be robust.</p> <p>(3) Incorporation of the above analysis into an inversion strategy.</p>			
14. SUBJECT TERMS scattering, electromagnetic, magnetotelluric (MT)			15. NUMBER OF PAGES
			16. PRICE CODE
17. SECURITY CLASSIFICATION OF REPORT Unclassified	18. SECURITY CLASSIFICATION OF THIS PAGE Unclassified	19. SECURITY CLASSIFICATION OF ABSTRACT Unclassified	20. LIMITATION OF ABSTRACT UL

19980511 070

DTIC QUALITY INSPECTED 3

Final Technical Report
Pulse Propagation in Random Media F 49620-95-1-0137
95/02/01 - 98/01/31

The research conducted during this period was initially done in collaboration with George Papanicolaou (Stanford University) and Benjamin White (Exxon Research & Engineering Co.) During the last half of this time period, however, the work was done in collaboration with Benjamin White and Leonard Srnka (Exxon Exploration Co.). In broad terms, the work focused upon direct and inverse problems involving wave propagation in complex heterogeneous media, modeled as random media. More specifically, the work has focused upon the following areas:

- (1) Multiple scattering of electromagnetic waves in randomly layered dissipative media. The magnetotelluric (MT) problem considered has lent itself to modeling within the "weak noise" or Gauss Markov regime. In addition to considering propagation per se, the issue of the detection of anomalous layers has been addressed. Details are presented in the enclosed preprint, "Random Scattering in Magnetotellurics", by Benjamin White, Werner Kohler and Leonard Srnka, which has been submitted for publication to Geophysics.
- (2) Extension of the ideas mentioned above to the case of an undulating (locally layered) medium. The theory developed for layered media is shown to be robust.
- (3) Incorporation of the above analysis into an inversion strategy.

1. Magnetotelluric Probing

We consider plane electromagnetic waves normally incident upon a layered Earth model in which the resistivity is assumed to vary with depth. This is the standard MT model. Very low frequencies are considered, i.e. $10^{-2} \leq f \leq 10^3$. At these low frequencies, skin depth is large and the incident EM energy is capable of penetrating to considerable depth. Certain substances, such as groundwater and hydrocarbons, have anomalously large resistivities while others, such as hot, pressurized brine, are very conducting. One of the problems we considered was the detection of such anomalous layers.

The main contribution of this work is our accounting for the effects of rapidly varying, fine scale resistivity variations. The problem falls within the theory developed by Khasminskii (Theory of Probability and its Applications, 11, 1966, p. 211-228). Using this theory, the surface impedance (measured at a number of discrete frequencies across the band of interest) is shown to be asymptotically described as a Gaussian random vector. The mean value of this vector is the "effective medium" impedance vector, i.e. it is the impedance vector one would measure were the randomly fluctuating resistivity replaced by a smooth effective medium. The covariance matrix of the surface impedance fluctuations is explicitly computable. The theory is robust and does not depend upon any detailed assumptions about the resistivity microstructure fluctuation statistics.

The Gaussian character of the limiting impedance statistics makes the signal processing aspects of the problem particularly tractable. For the problem we consider, a thin highly resistive layer is assumed to either be present or not at some depth. The task at hand is to use the measured surface impedance data to reach a decision. The Neyman-Pearson lemma provides the optimal test. As was mentioned, the Gaussian character of the limiting statistics makes this test relatively straightforward to implement.

Although the study conducted deals exclusively with the MT problem, the ideas are general in scope and would apply to other scenarios in which the underlying scales of the problem are similar. One application that might be considered is the problem posed by

Richard Albanese several years ago, in which the detection of buried chemical pools was the issue.

2. Locally Layered Media:

The effort here has been to extend the model to accommodate deviations from layering. Undulations are introduced and the goal is to both extend the relevant theory to this case and also, simultaneously, to demonstrate the robustness of the layered media results. For the acoustic problem studied at length in SIAM Review (December 1991, p. 519-625), this has been difficult; a number of false starts and dead ends have occurred. Moreover, the results obtained have proven too complicated to be useful.

For the simpler Gauss-Markov limit associated with the above-mentioned MT problem, however, the situation is simpler. Because of the scaling, a straightforward perturbation scheme can be used, as shown below, to account for the randomness and geometric undulations as additive effects. In fact, the effects of the randomness are ultimately computed using the plane-layered model since the effects of the undulations upon the randomness is of higher order.

Let δ denote a small parameter as in the preprint, representing the ratio of the microscale correlation length to the macroscale. Assume that the undulations are defined as level curves of $z' = z + \sqrt{\delta}Z(x, y, z)$, where Z is a known function. We introduce a new coordinate system of the form:

$$x' = x + \sqrt{\delta}X(x, y, z, \sqrt{\delta}), \quad y' = y + \sqrt{\delta}Y(x, y, z, \sqrt{\delta}), \quad z' = z + \sqrt{\delta}Z(x, y, z)$$

where X, Y must be determined so that x', y' are everywhere $\perp z'$. Assuming X, Y to possess expansions in powers of $\sqrt{\delta}$, these functions can be determined. (Generally, the x', y' coordinates cannot be chosen to be mutually orthogonal, however.) In terms of these new coordinates, we assume that the conductivity σ is a rapidly varying function of z' , i.e. $\sigma = \sigma(z'/\delta)$.

We can then derive equations for the electric and magnetic fields transverse to z' . The derivations are tedious but straightforward extensions of the ideas in Marcuvitz's Waveguide Handbook. We obtain:

$$\begin{aligned} \partial_{z'} E_{x'} &= \sigma^{-1} \partial_{x'} \left[\partial_{x'} H_{y'} - \partial_{y'} H_{x'} + \sqrt{\delta} (X_x \partial_{x'} H_{y'} - Y_y \partial_{y'} H_{x'} + X_{xy} H_{x'} - Y_{xy} H_{y'}) \right] + \\ &\sqrt{\delta} \sigma^{-1} (X_x - Z_z) \partial_{x'} (\partial_{x'} H_{y'} - \partial_{y'} H_{x'}) - \sqrt{\delta} Z_{xx} E_{x'} - \sqrt{\delta} \sigma^{-1} Z_{xz} (\partial_{x'} H_{y'} - \partial_{y'} H_{x'}) + \\ &i\omega\mu \left[\sqrt{\delta} (X_y + Y_x) H_{x'} + (1 - \sqrt{\delta} Z_z) H_{y'} \right] + O(\delta) \end{aligned}$$

$$\begin{aligned} \partial_{z'} E_{y'} &= \sigma^{-1} \partial_{y'} \left[\partial_{x'} H_{y'} - \partial_{y'} H_{x'} + \sqrt{\delta} (X_x \partial_{x'} H_{y'} - Y_y \partial_{y'} H_{x'} + X_{xy} H_{x'} - Y_{xy} H_{y'}) \right] + \\ &\sqrt{\delta} \sigma^{-1} (Y_y - Z_z) \partial_{x'} (\partial_{x'} H_{y'} - \partial_{y'} H_{x'}) - \sqrt{\delta} Z_{yy} E_{y'} - \sqrt{\delta} \sigma^{-1} Z_{yz} (\partial_{x'} H_{y'} - \partial_{y'} H_{x'}) - \\ &i\omega\mu \left[\sqrt{\delta} (X_y + Y_x) H_{y'} + (1 - \sqrt{\delta} Z_z) H_{x'} \right] + O(\delta) \end{aligned}$$

$$E_{z'} = \sigma^{-1} \left[\partial_{x'} H_{y'} - \partial_{y'} H_{x'} + \sqrt{\delta} (X_x \partial_{x'} H_{y'} - Y_y \partial_{y'} H_{x'} + X_{xy} H_{x'} - Y_{xy} H_{y'}) \right] + O(\delta)$$

Analogous equations for the magnetic field components are easily obtained by duality. Stacking the (locally) transverse field components into a 4×1 vector \bar{X} leads to the following equation structure:

$$\partial_z \bar{X} = \left[L_0 + \sqrt{\delta} \left(\frac{1}{\sqrt{\delta}} L_1 + L_2 \right) \right] \bar{X}$$

where L_0 is an $O(1)$ deterministic operator, $\frac{1}{\sqrt{\delta}} L_1$ is an appropriately scaled zero mean random operator arising from the random resistivity fluctuations and L_2 is a deterministic operator arising because of the undulations in the layering. To leading order, the effects of the undulations occur as an additive operator. Employing a perturbation expansion leads to an additive contribution due to the undulations at the level of the fields themselves. The leading order term corresponds to effective medium theory, the $O(\sqrt{\delta})$ correction associated with $\frac{1}{\sqrt{\delta}} L_1$ is the usual Gauss Markov correction associated with the layered randomness and the $O(\sqrt{\delta})$ correction associated with L_2 arises due to the undulations.

This simple structure leads to explicitly computable results. Computations are currently being done for representative geometries. The case where the lateral undulations are themselves random, but independent of and slowly-varying relative to the rapid random layering, is also being evaluated. When complete, the results will be submitted for publication.

3. Inversion:

The results discussed in (1), and presented in more detail in the enclosed preprint, lend themselves naturally to the problem of inversion. In this case, the surface impedance measurement data is used to infer the large scale subsurface resistivity structure (i.e. the effective medium resistivity). The contribution of the Gauss-Markov theory is to explicitly characterize the cross-correlations of the measured multi-frequency surface impedance noise.

Consider Maximum-Likelihood estimation. Because of the multivariate Gaussian character of the measured data, the task reduces to minimizing a quadratic functional of the form:

$$\left(\bar{X}_d - \bar{X}_m \right)^T C_m^{-1} \left(\bar{X}_d - \bar{X}_m \right) + \ln(\det C_m)$$

where \bar{X}_d is the measured data vector while \bar{X}_m and C_m represent the mean vector and covariance matrix corresponding to the particular model under consideration. In particular, if N layers (resting upon a semi-infinite basement) are being used in the model to attempt to fit the data, then \bar{X}_m and C_m are functions of $3N + 1$ variables, the length, mean conductivity and noise strength of each layer together with the basement conductivity. In Appendix A of the enclosed preprint, formulas are given that enable one to evolve the mean impedance as well as the covariance matrix across a layer. The explicit nature of these formulas enables one to similarly evolve the partial derivatives of these quantities with respect to the model parameters. In this way one obtains an explicit evaluation not only of the objective function at the current model state but also its gradient with respect to the model parameters.

These concepts have been developed and are currently being implemented. When complete, the results will be submitted for publication.

Publications:

“Localization and Mode Conversion for Elastic Waves in Randomly Layered Media I”, by W. Kohler, G. Papanicolaou and B. White, *Wave Motion*, vol. 23 (1996), pp. 1-22.

“Localization and Mode Conversion for Elastic Waves in Randomly Layered Media II”, by W. Kohler, G. Papanicolaou and B. White, *Wave Motion*, vol. 23 (1996), pp. 181-201.

“Localization of Low Frequency Elastic Waves”, by W. Kohler, G. Papanicolaou and B. White, *Stochastic Models in Geosystems*, edited by S. Molchanov and W. Woyczynski, Vol. 85, *IMA Volumes in Mathematics and its Applications*, 1997, pp. 209-217.

“Statistical Inversion from Reflections of Spherical Waves by a Randomly Layered Medium”, by M. Asch, W. Kohler, G. Papanicolaou, M. Postel and B. White, *Waves in Random Media*, vol. 6, (1996), pp. 293-334.

“Random Scattering in Magnetotellurics”, by Benjamin White, Werner Kohler and Leonard J. Srnka, submitted to *Geophysics*.

Presentations:

AFOSR workshop, San Antonio, January 1995

SIAM meeting, Kansas City, July 1996

SIAM meeting, Stanford, July 1997

AMS meeting, Albuquerque, November 1997

Students Receiving Support:

Lewis Buterakos received some support during summers of 1995 & 1996.

Karen Potanka and Steven Sinnott received some support during the summer of 1997.

RANDOM SCATTERING IN MAGNETOTELLURICS

BENJAMIN S. WHITE, WERNER E. KOHLER, AND LEONARD J. SRNKA

ABSTRACT. Typical well logs show substantial variations of formation electrical resistivity over small spatial scales, down to the resolution of the logging tool. Using a plane stratified Earth model, we examine the effects of this fine scale microstructure on scattering of the naturally occurring electromagnetic waves used in magnetotellurics (MT). We show theoretically how MT data may be viewed as arising largely from a smoothed "effective medium" version of the resistivity *vs.* depth profile. The difference between the data produced by the true medium and that produced by the effective medium is due to random scattering noise, which is fundamental to MT since it arises from the very small spatial scales that are usually ignored. This noise is substantial and has unique statistical properties, which we characterize. We examine the implications of the existence of this noise for the detectability of a thin layer of increased resistivity at depth. The theory is shown to agree well with Monte Carlo simulations.

1. INTRODUCTION

In magnetotelluric (MT) surveys [1], [2], [3], surface measurements of the Earth's electrical impedance over a broad frequency range at a number of different sites are analyzed to produce maps of electrical resistivity in the subsurface. Naturally occurring ambient electromagnetic (EM) radiation is used as a source. The method is widely used for the mapping of crustal-scale structures both on land and at the seafloor, and can also be useful for sedimentary basin exploration in areas where seismic reflection data quality is poor.

The principal drawback of MT is its limited accuracy and spatial resolution, due to the diffusive character of low frequency EM propagation in the Earth. Mathematically this is to be expected, since the processing of the MT surface measurements to produce a subsurface map is an inverse problem which is classically ill-posed in the sense of Hadamard [4]. That is, many different solutions can fit the observed data almost as well. In fact, EM prospecting was a seminal problem in inverse theory. Early research on EM prospecting was done by Tikhonov [5], [6], [7], [8] and Cagniard [9]; the theoretical aspects of the inverse problem were later studied by Weidelt [10]. Tikhonov, in particular [5], showed that, contrary to prevailing wisdom, ill-posed problems could be solved both theoretically and in practice (for a history, see [2], Chapter 1). Today, the Tikhonov regularization technique has achieved great success in solving inverse problems in many diverse scientific fields [11].

The basic assumption of regularization theory is that the solution is piecewise smooth. In choosing among candidate solutions, smoothness is valued in addition to the candidate's ability to explain the data, and it is this additional criterion that allows a "best" solution to be found. In the words of Parker [12] (p. 294), "we seek the simplest, least exciting kind of solution".

The second author was supported by Air Force grant F49620-95-1-0137.

We thank Exxon Exploration Company for permission to release the induction log data.

However, the smoothness assumption is clearly false for MT, as is evident from even a casual inspection of well logs. As an example, Figure 1 shows formation resistivity as a function of depth for an onshore Louisiana oil exploration well in the Gulf of Mexico basin. The lithology consists primarily of intermixed layers of sandstone and shale. Note that the geologic section is quite conductive, which is typical for this basin. The data were recorded using an Atlas Wireline DIFL induction logging tool (RILD response), with a nominal two foot vertical resolution. The figure illustrates the well known fact that formation resistivity is rapidly varying on very small spatial scales down to the spatial resolution of the tool. Furthermore, the amplitude of the resistivity fluctuations is by no means small. In general, resistivities varying rapidly over one or more orders of magnitude are not uncommon in well log data. In this paper we examine the effects of this fine scale structure on EM scattering, and the subsequent implications for the fundamental limits of vertical resolution in MT data processing.

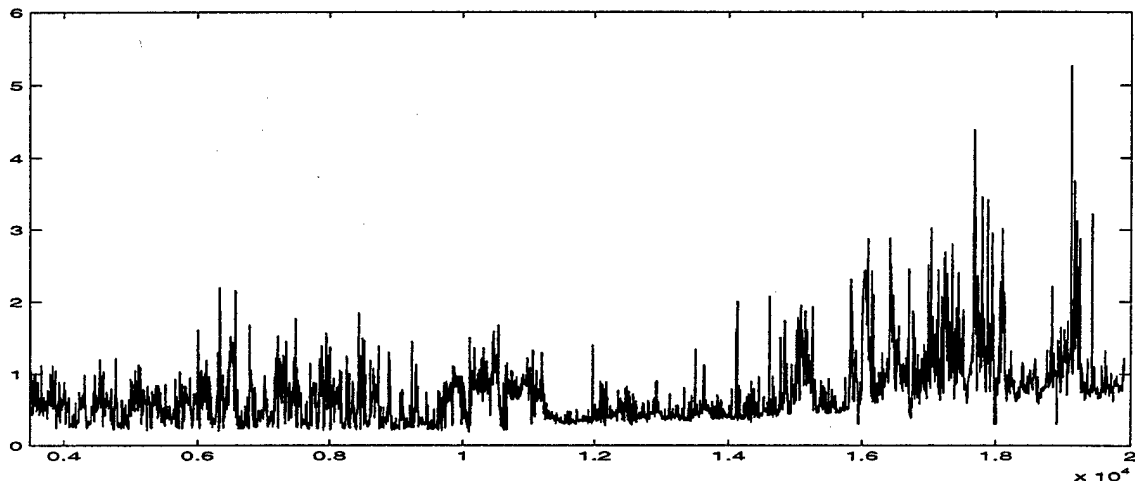


FIGURE 1. Onshore Louisiana Well Log Data: Resistivity (Ohm-m) vs. Depth (ft).
The record extends from 3,500 ft to 19,900 ft in depth.

It is natural to describe the small scale resistivity fluctuations as a random process called the microstructure. An MT survey will not recover resistivity with all the resolution of the microstructure, but only some kind of smoothed, spatially averaged, version. This idea will be made more precise below, where furthermore we show that it is conductivity, *i.e.* the reciprocal of resistivity, that is averaged. But to explore the spatial scales involved, consider a sliding window with a length of 500 ft centered at different depths in Figure 1. As the center of the window moves along the abscissa in Figure 1, the average resistivity over that window changes smoothly. Besides the average, other estimated statistics will also vary with window position. As a typical example, Figure 2 shows the normalized resistivity autocorrelation function, estimated from a 500 ft window centered at a depth of 4,450 ft. From this figure, the length scale of the microstructure can be estimated as about $\bar{l} = 13$ ft (nominally 4 m). This is the microscale, *i.e.*, the correlation length of the microstructure; two points separated by much more than 4 m will have resistivity fluctuations that are not significantly correlated, while significant correlations will exist for distances much smaller than this. Our studies of other portions of this log, and of other resistivity logs with different lithologies, have produced qualitatively similar results.

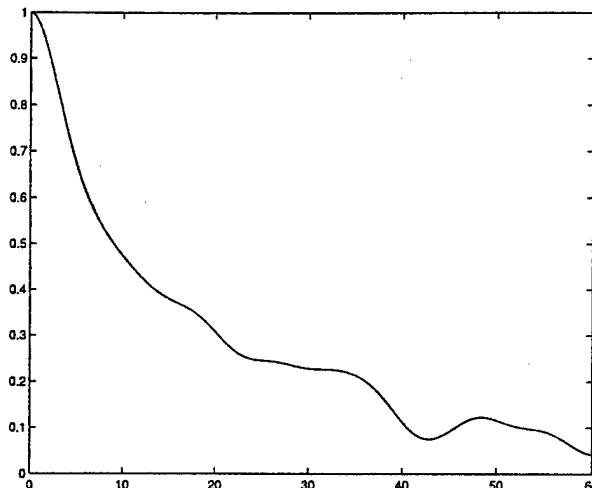


FIGURE 2. Typical Onshore Louisiana Well Log Autocorrelation Function: Normalized Resistivity Autocorrelation *vs.* Lag (ft), measured over a 500 ft window centered at a depth of 4,450 ft.

This value of \tilde{l} is consistent with studies of acoustic well logs, which, while recording a different material property, may be expected to vary on the same spatial scale. In reflection seismology, scattering from thin beds is explained by the now classical theory of O'Doherty and Anstey [13]. Their Figure 11 shows an autocorrelation function of reflectivities that is at least qualitatively consistent with an exponential autocorrelation function of acoustic impedance, and a correlation length \tilde{l} of a few meters. Godfrey *et. al.* [14] and Banik *et. al.* [15] use decreasing exponentials to get good data fits to the autocorrelation function, and give explanations for the observed exponential behavior in terms of Markovian models for the sedimentation process. Banik *et. al.* cite a typical exponential decay length, corresponding to our \tilde{l} , of 4.5 m. White *et. al.* [16] also found autocorrelation functions that were well fit by exponentials, with \tilde{l} varying between 1 m and 10 m, and a most typical value of about 3 m. Other studies of the statistics of acoustic well logs that are generally consistent with these results are reported by Walden and Hosken [17], Velzeboer [18], and Sato [19]. Some of the larger values of \tilde{l} obtained by these authors have been up to 20 m. A review of the mathematics of acoustic scattering in stratified media with fine scale structure is given by Asch *et. al.* [20].

In what follows, we consider horizontally plane stratified media, so that resistivity varies as a function of depth only. Besides the microscale \tilde{l} , we consider a macroscale \tilde{L} , on which significant variations of resistivity might be recovered by MT. The resistivity is then modeled as a function of these two disparate spatial scales $\tilde{L} \gg \tilde{l}$. The ratio $\delta = \tilde{l}/\tilde{L}$ is a small parameter which is used in the asymptotic analysis that follows.

In Section 2 we show under wide hypotheses that, despite the microstructure, there is a piecewise smooth resistivity *vs.* depth curve that approximately explains the data. More specifically, we use a theorem of Khasminskii [21] to derive "effective medium theory" — *i.e.* we construct, by suitable averaging, a smooth, effective medium which will produce surface impedance measurements that match those produced by the true resistivity profile, but with a small error of order $O(\sqrt{\delta})$. In this context, the ill-posedness of the inverse problem can be seen as a consequence of effective

medium theory. Since many different microstructures can be smoothed to produce the same effective medium, it is not possible to distinguish between these different microstructures, as a complete inversion algorithm would have to do. The inverse problem becomes well-posed if one solves for the effective medium only. However in this case the data cannot match the solution of the forward problem, but will be in error by an amount of order $O(\sqrt{\delta})$.

This order $O(\sqrt{\delta})$ error in the data is a kind of “geologic noise” caused by multiple scattering from the fine scale microstructure. This noise is fundamental to MT and cannot be reduced by instrumentation, since it is produced solely by a discrepancy between the true resistivity *vs.* depth profile and the smooth curve that is assumed in the mathematical inversion. Moreover, this kind of scattering noise can be substantial. In Section 4 (See Figure 3) we compare an estimate of the magnitude of geologic noise to that of all other sources of error, based on an analysis of Parker [12], and find that, except for very low frequencies, the magnitudes are comparable.

In Section 2 we also apply another theorem of Khasminskii’s [21] to characterize the unique statistical properties of geologic scattering noise. Further formulas for the effective calculation of these statistics are developed in Section 3. These statistics do not depend on the details of the microstructure, but only on some averaged quantities. Furthermore, because Khasminskii’s theorem is a kind of Central Limit Theorem for differential equations, the surface impedance scattering noise has a Gaussian distribution even when the resistivity fluctuations do not. Thus there is a good deal of model independence, and it is not necessary to undertake a detailed statistical analysis of the Earth’s resistivity microstructure in order to apply the theory. In particular, for the case of a homogeneous half space containing random fluctuations (*i.e.* a random half space), we can derive explicit algebraic formulas that predict the variances and covariances of the real and imaginary parts of an array of surface impedances measured at different frequencies. These formulas depend only on a single microstructure parameter which characterizes the noise strength and merely scales all the variances and covariances. Thus, for a homogeneous random half space, the statistics are universal.

In Section 4 we study the implications of the theory for the detectability of a thin layer of material in the subsurface, when the material’s resistivity varies markedly from that of the background, as in prospecting for hydrocarbons. Ultimately, detectability is also a question of spatial resolution for MT, since very large amounts of the material will almost certainly be detected, while very small amounts will almost certainly be missed. Clearly, detectability also depends on the depth of investigation.

The question then is, “At a given depth, how strong a target is necessary for detection, given that the EM waves used as a probe are scattered by the microstructure ?” In Section 4 we develop the theory for a model problem of this type. We show that there is an optimal method of data processing, based on the Neyman-Pearson lemma [22], [23]. Attempts at detection will make two types of errors: false positives (“detecting” a nonexistent target) and false negatives (failing to detect a target). These two types of errors cannot be eliminated, but can be traded off against each other by setting a threshold on how compelling the evidence needs to be for detection to be declared. We derive expressions for this tradeoff, *i.e.* expressions relating the false negative rate to the false positive rate. As is standard practice in detection theory [23], this relation between error

rates can be expressed as a ROC (Receiver Operating Characteristic) curve, which is a plot of the probability of successful detection *vs.* the false positive rate. Because the method is theoretically optimal, its ROC curve cannot be improved, and so provides a fundamental limit to detectability.

In Section 5, we compare the theory to Monte Carlo simulations. We obtain excellent agreement of the simulations and the theoretical noise statistics over a frequency range spanning five orders of magnitude. For the detectability theory we include both geologic scattering noise and a white noise component, to model other sources of error. The detectability theory also compares well with simulations.

Although we have not pursued the idea in this paper, knowledge of the noise statistics should be of direct value in the inversion of MT data, by suggesting the theoretically optimal misfit function to be used in optimization. A simple example, corresponding to current practice, is the use of variance-weighted least squares [12], [24]. This misfit function is appropriate if the data errors at each frequency are uncorrelated, but have different variances. However, for geologic scattering noise, the errors at different frequencies are highly correlated, as we show here. So the appropriate misfit function should be a quadratic form in the errors, weighted by all the elements of the inverse of the covariance matrix. Whether substantial improvement in inversions can be obtained using this misfit function is a subject for future research.

2. SPATIAL SCALES AND A STOCHASTIC LIMIT

We consider a plane stratified Earth occupying the half space $z \leq 0$, with a basement layer consisting of a homogeneous half space for $z < -L$ and with air in $z > 0$. Let σ be conductivity, μ the magnetic permeability, ϵ the dielectric permittivity, \mathbf{E} the electric field and \mathbf{H} the magnetic field. μ will be assumed to be constant while σ and ϵ will be assumed to vary with z , but not with frequency. For angular frequency ω and time dependence $e^{-i\omega t}$, Maxwell's equations become

$$\begin{aligned}\nabla \times \mathbf{E} &= i\omega\mu\mathbf{H} \\ \nabla \times \mathbf{H} &= (\sigma - i\omega\epsilon)\mathbf{E}.\end{aligned}\tag{2.1}$$

For a normally incident plane wave (with x -directed electric field and y -directed magnetic field), we obtain the usual equations for the scalar components E and H

$$\begin{aligned}\frac{\partial}{\partial z}E &= -i\omega\mu H \\ \frac{\partial}{\partial z}H &= (\sigma - i\omega\epsilon)E.\end{aligned}\tag{2.2}$$

To nondimensionalize, we choose typical constants $\tilde{\mu}$, $\tilde{\epsilon}$, $\tilde{\omega}$, $\tilde{\sigma}$, \tilde{H} and define a typical length scale \tilde{L} , impedance $\tilde{\xi}$ and reference electric field strength \tilde{E} by

$$\begin{aligned}\tilde{L} &= 1/\sqrt{\tilde{\omega}\tilde{\mu}\tilde{\sigma}} \\ \tilde{\xi} &= 1/\tilde{\sigma}\tilde{L} \\ \tilde{E} &= \tilde{\xi}\tilde{H}.\end{aligned}\tag{2.3}$$

Note that $\sqrt{2\tilde{L}}$ is the skin depth. Let the impedance be

$$\xi = E/H.\tag{2.4}$$

Magnetotelluric surveys produce measurements of ξ at $z = 0$ over a range of frequencies ω .

Set

$$\begin{aligned} z' &= z/\tilde{L}, & \mu' &= \mu/\tilde{\mu}, & \epsilon' &= \epsilon/\tilde{\epsilon}, & \omega' &= \omega/\tilde{\omega} \\ H' &= H/\tilde{H}, & E' &= E/\tilde{E}, & \xi' &= \xi/\tilde{\xi}. \end{aligned} \quad (2.5)$$

Then equations (2.2) and (2.4) hold again for the primed variables.

In what follows, we use the nondimensional variables but, for notational convenience, drop the primes. Also, for $z \leq 0$, the parameter regimes to be considered will permit us to employ the usual quasi-static approximation [2]; that is, displacement currents are neglected so that effectively ϵ may be set equal to 0. Then, substitution of (2.4) into (2.2) yields

$$\frac{\partial}{\partial z} \xi = -\sigma \xi^2 - i\omega\mu, \quad z < 0. \quad (2.6)$$

Because of the continuity of E and H , ξ is also continuous across layer boundaries. The condition that there are no outgoing waves in $z < -L$ yields that

$$E = \xi_B H \quad \text{at } z = -L, \quad (2.7)$$

where

$$\begin{aligned} \xi_B &= \frac{\omega\mu_B}{k_B} \\ k_B &= \sqrt{\frac{\omega\mu_B\sigma_B}{2}} \left(\frac{1+i}{2} \right). \end{aligned} \quad (2.8)$$

Thus, an initial condition for (2.6) is

$$\xi = \xi_B \quad \text{at } z = -L. \quad (2.9)$$

We take permeability to be constant and consider variations in the conductivity. In particular, we consider deterministic macroscale variations of the conductivity on a spatial scale of order \tilde{L} , and random microscale variations on a much smaller spatial scale $\tilde{l} \ll \tilde{L}$. Let

$$\delta = \tilde{l}/\tilde{L} \ll 1, \quad (2.10)$$

so that in dimensional units, $\sigma = \sigma(z/\tilde{l}, z/\tilde{L})$. Then in nondimensional units, $z' = z/\tilde{L}$. We obtain, after again dropping primes for notational convenience, that

$$\sigma = \sigma(z/\delta, z). \quad (2.11)$$

The random function $\sigma(z_1, z_2)$ now drives equation (2.6) stochastically, with $z_1 = z/\delta$, $z_2 = z$. We assume that, for each fixed z_2 , $\sigma(z_1, z_2)$ is a stochastic process in z_1 which satisfies a *mixing condition*. This means that $\sigma(z_1 + \Delta z_1, z_2)$ becomes statistically independent of $\sigma(z_1, z_2)$ as the microscale separation distance $\Delta z_1 \rightarrow \infty$. In other words, we assume that the microstructure has no long-range correlations. Other technical conditions are given by Khasminskii [21], whose theorems we will now apply.

Let $\xi_1, \xi_2, \dots, \xi_N$ be N impedances corresponding, respectively, to the N frequencies $\omega_1, \omega_2, \dots, \omega_N$. We will compute their joint statistics, approximately, for small δ . Let

$$\begin{aligned} \xi_j^R &= \Re\{\xi_j\} \\ \xi_j^I &= \Im\{\xi_j\}, \quad j = 1, 2, \dots, N. \end{aligned} \quad (2.12)$$

We define the vector $\mathbf{X} \in \mathbb{R}^{2N+1}$ by

$$\mathbf{X} = (\xi_1^R, \xi_2^R, \dots, \xi_N^R, \xi_1^I, \xi_2^I, \dots, \xi_N^I, z)^T. \quad (2.13)$$

Then, equation (2.6) for the complex impedance ξ implies that \mathbf{X} satisfies a vector stochastic differential equation of the form

$$\frac{d}{dz}\mathbf{X} = \mathbf{F}(z/\delta, \mathbf{X}), \quad \mathbf{X}(-L) = \mathbf{X}_0. \quad (2.14)$$

Here

$$\mathbf{X}_0 = (\xi_{B,1}^R, \dots, \xi_{B,N}^R, \xi_{B,1}^I, \dots, \xi_{B,N}^I, -L)^T, \quad (2.15)$$

where $\xi_{B,j}^R, \xi_{B,j}^I$ are the real and imaginary parts of ξ_B , given by (2.8), for frequency ω_j , and

$$\begin{aligned} \mathbf{F}(s, \mathbf{X}) &= \sigma(s, \mathbf{X}_{2N+1})\mathbf{H}(\mathbf{X}) + \mathbf{V} \\ \mathbf{H}(\mathbf{X}) &= ((\xi_1^R)^2 - (\xi_1^I)^2, \dots, (\xi_N^R)^2 - (\xi_N^I)^2, 2\xi_1^R\xi_1^I, \dots, 2\xi_N^R\xi_N^I, 0)^T \\ \mathbf{V} &= (0, \dots, 0, -\omega_1\mu, \dots, -\omega_N\mu, 1)^T. \end{aligned} \quad (2.16)$$

Equation (2.14) is of the type considered by Khasminskii [21]. To apply his Theorem (1.1), we compute

$$\bar{\mathbf{F}}(\mathbf{X}) = \lim_{z \rightarrow \infty} \frac{1}{z} \int_0^\infty E\{\mathbf{F}(s, \mathbf{X})\} ds, \quad (2.17)$$

where $E\{\cdot\}$ denotes expected or mean value. The deterministic function $\bar{\mathbf{F}}(\mathbf{X})$ is the average, both in probability and space (over the microstructure only), of $\mathbf{F}(s, \mathbf{X})$. Then, by Theorem (1.1) \mathbf{X} may be approximated, to leading order as $\delta \downarrow 0$, by the nonrandom vector $\bar{\mathbf{X}}$, which satisfies

$$\begin{aligned} \frac{d}{dz}\bar{\mathbf{X}} &= \bar{\mathbf{F}}(\bar{\mathbf{X}}) \\ \bar{\mathbf{X}}(-L) &= \mathbf{X}_0. \end{aligned} \quad (2.18)$$

Equation (2.18) is equivalent to effective medium theory. To see this, note from (2.16) that $\bar{\mathbf{F}}$ is obtained from \mathbf{F} by replacing the random process $\sigma(s, z)$ by its local average over the microstructure, $\bar{\sigma}(z)$, where

$$\bar{\sigma}(z) = \lim_{s \rightarrow \infty} \frac{1}{s} \int_0^s E\{\sigma(s', z)\} ds'. \quad (2.19)$$

Therefore, each ξ_j is approximated, to leading order, by the deterministic impedance $\bar{\xi}_j$ which satisfies

$$\begin{aligned} \frac{d}{dz}\bar{\xi}_j &= -\bar{\sigma}(z)\bar{\xi}_j^2 - i\omega_j\mu, \quad -L < z < 0 \\ \bar{\xi}_j(-L) &= \xi_{B,j} \end{aligned} \quad (2.20)$$

Note that $\bar{\sigma}$, and hence $\bar{\xi}_j$, vary only on the macroscale since the local averaging (2.19) has erased all microscale variation.

To derive corrections to effective medium theory, we next apply Khasminskii's Theorem (3.1). Let

$$\mathbf{Y} = \frac{1}{\sqrt{\delta}}(\mathbf{X} - \bar{\mathbf{X}}). \quad (2.21)$$

Then as $\delta \downarrow 0$, the statistics of \mathbf{Y} are well-approximated by the statistics of \mathbf{Y}^0 , where \mathbf{Y}^0 is a Gaussian random process that satisfies the linear integral equation

$$\mathbf{Y}^0(z) = \mathbf{W}^0(z) + \int_{-L}^z \frac{\partial}{\partial \bar{\mathbf{X}}} \bar{\mathbf{F}}(\bar{\mathbf{X}}(\zeta)) \mathbf{Y}^0(\zeta) d\zeta. \quad (2.22)$$

Here $\mathbf{W}^0(z)$ is a Gaussian process with independent increments, zero expectation and a correlation matrix

$$E\{(\mathbf{W}^0(z)) (\mathbf{W}^0(z))^T\} = \int_{-L}^z \mathbf{A}(\bar{\mathbf{X}}(\zeta)) d\zeta, \quad (2.23)$$

where

$$\mathbf{A}(\mathbf{X}) = \lim_{z \rightarrow \infty} \frac{1}{z} \int_0^z \int_0^z E\{[\mathbf{F}(s_1, \mathbf{X}) - \bar{\mathbf{F}}(\mathbf{X})] [\mathbf{F}(s_2, \mathbf{X}) - \bar{\mathbf{F}}(\mathbf{X})]^T\} ds_1 ds_2. \quad (2.24)$$

From (2.16), (2.24) we obtain that

$$\mathbf{A}(\mathbf{X}) = \gamma^2(\mathbf{X}_{2N+1}), \mathbf{H}(\mathbf{X}) \mathbf{H}(\mathbf{X})^T, \quad (2.25)$$

where

$$\gamma^2(z) = \lim_{s \rightarrow \infty} \frac{1}{s} \int_0^s \int_0^s E\{(\sigma(s_1, z) - \bar{\sigma}(z)) (\sigma(s_2, z) - \bar{\sigma}(z))\} ds_1 ds_2. \quad (2.26)$$

A more convenient representation for the correction term is obtained by expressing $\mathbf{W}^0(z)$ as an Ito stochastic integral [25]

$$\mathbf{W}^0(z) = \int_{-L}^z \gamma(\zeta) \mathbf{H}(\mathbf{X}(\zeta)) d\beta(\zeta), \quad (2.27)$$

where $\beta(z)$ is a standard Brownian motion (the Wiener process). Using the “white noise”-like property of the Brownian differential

$$E\{d\beta(\zeta_1) d\beta(\zeta_2)\} = \delta(\zeta_1 - \zeta_2) d\zeta_1, \quad (2.28)$$

(where $\delta(\zeta_1 - \zeta_2)$ is the standard δ -function). We may verify that \mathbf{W}^0 defined by (2.27) has the required covariance (2.23).

Using (2.27), equation (2.22) can be differentiated to give a set of Ito stochastic differential equations, *i.e.* “white noise” equations. We identify the corrections as

$$\mathbf{Y}^0 = \left(\hat{\xi}_1^R, \dots, \hat{\xi}_N^R, \hat{\xi}_1^I, \dots, \hat{\xi}_N^I, 0 \right)^T, \quad (2.29)$$

so that, from (2.21) written in component form, we obtain

$$\xi_j(z) = \bar{\xi}_j(z) + \sqrt{\delta} \hat{\xi}_j(z). \quad (2.30)$$

The equations for the $\hat{\xi}_j$ are

$$\begin{aligned} d\hat{\xi}_j &= -2\bar{\sigma}(z) \bar{\xi}_j(z) \hat{\xi}_j(z) dz + \gamma(z) \bar{\xi}_j^2(z) d\beta(z) \\ \hat{\xi}_j(-L) &= 0. \end{aligned} \quad (2.31)$$

Thus, the $\hat{\xi}_j$ are linear “white noise” perturbations of (2.20). In fact, (2.31) can be derived heuristically by substituting (2.30) into (2.6), assuming that $\bar{\xi}_j$ satisfies the effective medium equations

(2.20). Then, one obtains, to order $O(\sqrt{\delta})$

$$\frac{d}{dz} \hat{\xi} \approx -2\sigma(z/\delta, z) \bar{\xi} \hat{\xi} - \frac{[\sigma(z/\delta, z) - \bar{\sigma}(z)]}{\sqrt{\delta}} \bar{\xi}^2. \quad (2.32)$$

Equation (2.31) is obtained from (2.32) by replacing the first $\sigma(z/\delta, z)$ by its average and by identifying $[\sigma(z/\delta, z) - \bar{\sigma}(z)]/\sqrt{\delta}$ as an appropriate white noise with covariance proportional to $\gamma^2(z)$, which is the "effective noise strength" of the microstructure at macroscopic position z .

To summarize, the conductivity is first averaged locally, via (2.19), and the result is used to compute the impedance $\bar{\xi}$, in the effective medium of conductivity $\bar{\sigma}(z)$, via equation (2.20). The leading order correction, obtained via (2.30), is of order $O(\sqrt{\delta})$, and is given by the $\hat{\xi}_j$, which satisfy the Ito stochastic differential equations (2.31). We shall next use (2.31) to compute the joint statistics of the $\hat{\xi}_j$.

3. RANDOM SCATTERING STATISTICS: PROPAGATION EQUATIONS AND A HOMOGENEOUS RANDOM HALF-SPACE

From equation (2.31), it follows that the $\hat{\xi}_j$ are zero mean, jointly Gaussian random variables, and so it remains to compute their covariances at $z = 0$ to determine the statistics of the impedance fluctuations at the surface due to multiple scattering from the microstructure. Let

$$\begin{aligned} C_{jl}^{RR} &= E\{\hat{\xi}_j^R \hat{\xi}_l^R\}, & C_{jl}^{II} &= E\{\hat{\xi}_j^I \hat{\xi}_l^I\} \\ C_{jl}^{RI} &= E\{\hat{\xi}_j^R \hat{\xi}_l^I\}, & C_{jl}^{IR} &= C_{lj}^{RI}, \quad j, l = 1, 2, \dots, N. \end{aligned} \quad (3.1)$$

Let $*$ denote complex conjugate. We will determine the real matrices in (3.1) from the two complex matrices

$$\hat{C}_{jl} = E\{\hat{\xi}_j \hat{\xi}_l\}, \quad \bar{C}_{jl} = E\{\hat{\xi}_j \hat{\xi}_l^*\}. \quad (3.2)$$

Note the symmetry properties; \hat{C} is complex symmetric and \bar{C} is Hermitian.

$$\hat{C}^T = \hat{C}, \quad \bar{C}^{*T} = \bar{C}. \quad (3.3)$$

Then, from the identity $\hat{\xi}_j = \hat{\xi}_j^R + i\hat{\xi}_j^I$ we obtain

$$\begin{aligned} C^{RR} &= \frac{1}{2} \Re\{\hat{C} + \bar{C}\}, & C^{II} &= \frac{1}{2} \Re\{\bar{C} - \hat{C}\} \\ C^{RI} &= \frac{1}{2} \Im\{\hat{C} - \bar{C}\}, & C^{IR} &= \frac{1}{2} \Im\{\hat{C} + \bar{C}\}. \end{aligned} \quad (3.4)$$

To derive an equation for \hat{C} , we use Ito's multiplication table [25], Table 1.

	$d\beta$	dz
$d\beta$	dz	0
dz	0	0

Table 1. Ito's Multiplication Table

Then

$$d(\hat{\xi}_j \hat{\xi}_l) = \hat{\xi}_l d\hat{\xi}_j + \hat{\xi}_j d\hat{\xi}_l + d\hat{\xi}_j d\hat{\xi}_l. \quad (3.5)$$

In the stochastic calculus, the extra term $d\hat{\xi}_j d\hat{\xi}_l$ is not zero since $(d\beta)^2 = dz$ according to Table 1. Substituting from (2.30) into (3.5) we obtain

$$d\left(\hat{\xi}_j \hat{\xi}_l\right) = -2\bar{\sigma} (\bar{\xi}_j + \bar{\xi}_l) \hat{\xi}_j \hat{\xi}_l dz + \gamma \left(\hat{\xi}_l \bar{\xi}_j^2 + \hat{\xi}_j \bar{\xi}_l^2\right) d\beta + \gamma^2 \bar{\xi}_j^2 \bar{\xi}_l^2 dz. \quad (3.6)$$

Now, taking expected values in (3.6), and using $E\{d\beta\} = 0$, we obtain

$$\begin{aligned} \frac{d}{dz} \hat{C}_{jl}(z) &= -2\bar{\sigma} (\bar{\xi}_j + \bar{\xi}_l) \hat{C}_{jl} + \gamma^2 \bar{\xi}_j^2 \bar{\xi}_l^2 \\ \hat{C}_{jl}(-L) &= 0. \end{aligned} \quad (3.7)$$

The initial condition in (3.7) follows from (2.31), i.e. the absence of random fluctuations at $z = -L$.

Similarly, from the stochastic differential

$$d\left(\hat{\xi}_j \hat{\xi}_l^*\right) = \hat{\xi}_l^* d\hat{\xi}_j + \hat{\xi}_j d\hat{\xi}_l^* + (d\hat{\xi}_j)(d\hat{\xi}_l^*) \quad (3.8)$$

we obtain

$$\begin{aligned} \frac{d}{dz} \bar{C}_{jl}(z) &= -2\bar{\sigma} (\bar{\xi}_j + \bar{\xi}_l^*) \bar{C}_{jl} + \gamma^2 \bar{\xi}_j^2 (\bar{\xi}_l^*)^2 \\ \bar{C}_{jl}(-L) &= 0. \end{aligned} \quad (3.9)$$

As an important special case, consider a homogeneous random half space, $z \leq 0$. Then $\bar{\sigma}$ and γ are constants and we can let $L \rightarrow \infty$. In this case, the initial conditions are ignored and the z -independent solutions for \hat{C} and \bar{C} are found from (3.7) and (3.9) to be

$$\hat{C}_{jl} = \left(\frac{\gamma^2}{2\bar{\sigma}}\right) \left(\frac{\bar{\xi}_j^2 \bar{\xi}_l^2}{\bar{\xi}_j + \bar{\xi}_l}\right), \quad \bar{C}_{jl} = \left(\frac{\gamma^2}{2\bar{\sigma}}\right) \left(\frac{\bar{\xi}_j^2 (\bar{\xi}_l^*)^2}{\bar{\xi}_j + \bar{\xi}_l^*}\right). \quad (3.10)$$

To determine $\bar{\xi}_j$ we may set $d\bar{\xi}_j/dz = 0$ in (2.20) to get an algebraic relation for $\bar{\xi}_j^2$; we obtain

$$\bar{\xi}_j^{hom} = \sqrt{\frac{\omega_j \mu}{\bar{\sigma}}} e^{-i\pi/4} \quad (3.11)$$

Substitution of (3.11) into (3.10) yields

$$\begin{aligned} \hat{C}_{jl}^{hom} &= \left(\frac{\gamma^2 \mu^{3/2}}{2^{3/2} \bar{\sigma}^{5/2}}\right) \left(\frac{\omega_j \omega_l}{\sqrt{\omega_j} + \sqrt{\omega_l}}\right) (-1 - i) \\ \bar{C}_{jl}^{hom} &= \left(\frac{\gamma^2 \mu^{3/2}}{2^{3/2} \bar{\sigma}^{5/2}}\right) \left(\frac{\omega_j \omega_l [(\sqrt{\omega_j} + \sqrt{\omega_l}) + i(\sqrt{\omega_j} - \sqrt{\omega_l})]}{\omega_j + \omega_l}\right). \end{aligned} \quad (3.12)$$

Substitution of (3.12) into (3.4) yields

$$\begin{aligned} C_{jl}^{RR(hom)} &= \alpha_{jl} \sqrt{\omega_j \omega_l}, & C_{jl}^{II(hom)} &= \alpha_{jl} (\omega_j + \omega_l + \sqrt{\omega_j \omega_l}) \\ C_{jl}^{RI(hom)} &= -\alpha_{jl} \omega_j, & C_{jl}^{IR(hom)} &= -\alpha_{jl} \omega_l, \end{aligned} \quad (3.13)$$

where

$$\alpha_{jl} = \left(\frac{\gamma^2 \mu^{3/2}}{2^{3/2} \bar{\sigma}^{5/2}}\right) \left(\frac{\omega_j \omega_l}{(\omega_j + \omega_l)(\sqrt{\omega_j} + \sqrt{\omega_l})}\right). \quad (3.14)$$

Traditionally, magnetotelluric data has been displayed in terms of the apparent resistivity [1]

$$\rho_a = \frac{|\xi|^2}{\omega \mu}, \quad (3.15)$$

where ξ is evaluated at the surface $z = 0$.

Substitution of (2.29) into (3.15) yields

$$\rho_a \approx \bar{\rho}_a + \sqrt{\delta} \hat{\rho}_a, \quad (3.16)$$

where

$$\bar{\rho}_a = \frac{|\bar{\xi}|^2}{\omega\mu} \quad (3.17)$$

$$\hat{\rho}_a = \frac{2\Re[\bar{\xi}^*\hat{\xi}]}{\omega\mu}. \quad (3.18)$$

From (3.18) we can compute the covariance of ρ_a at two different frequencies, ω_j and ω_l , as

$$E\{\hat{\rho}_{a,j}\hat{\rho}_{a,l}\} = \left(\frac{2}{\omega_j\omega_l\mu^2}\right) \Re\{\bar{\xi}_j^*\bar{\xi}_l^*\hat{C}_{jl} + \bar{\xi}_j^*\bar{\xi}_l\bar{C}_{jl}\}. \quad (3.19)$$

To evaluate (3.17), (3.19) for a homogeneous random half space, put (3.11) into (3.17) to obtain

$$\bar{\rho}_a^{hom} = \frac{1}{\bar{\sigma}}. \quad (3.20)$$

That is, $\bar{\rho}_a^{hom}$ is independent of frequency and equals the resistivity of the effective medium. However, the random fluctuations in apparent resistivity are not independent of frequency. Substitution of (3.12) into (3.17) yields

$$E\{\hat{\rho}_{a,j}^{hom}\hat{\rho}_{a,l}^{hom}\} = \gamma^2 \sqrt{\frac{\mu\omega_j\omega_l}{2\bar{\sigma}^7}} \left(\frac{1}{(\sqrt{\omega_j} + \sqrt{\omega_l})} + \frac{(\sqrt{\omega_j} + \sqrt{\omega_l})}{(\omega_j + \omega_l)} \right). \quad (3.21)$$

In particular, for $\omega_j = \omega_l = \omega$ we obtain the variance of $\hat{\rho}_a^{hom}$

$$E\{(\hat{\rho}_a^{hom})^2\} = \frac{3\gamma^2}{2} \sqrt{\frac{\mu\omega}{2\bar{\sigma}^7}}. \quad (3.22)$$

The variance increases as the square root of frequency, and so is zero at $\omega = 0$. This can be understood as resulting from an averaging over lengths of the order of a skin depth

$$z_s = \sqrt{\frac{2}{\omega\mu\sigma}}. \quad (3.23)$$

As frequency decreases, skin depth increases and the wave averages over more microstructure. Consequently, the variance decreases; effective medium theory becomes more accurate. Inserting (3.23) into (3.22) yields

$$E\{(\hat{\rho}_a^{hom})^2\} = \frac{3\gamma^2}{2\bar{\sigma}^4 z_s}. \quad (3.24)$$

The variance is thus inversely proportional to skin depth and proportional to noise strength γ^2 . The $\bar{\sigma}^{-4}$ dependence then follows from dimensional analysis.

The homogeneous random half space enables us to study the effects of random conductivity fluctuations in a setting free of any macroscale artifacts. How important are these fluctuations as a source of error?

Parker [12], in Table 5.02A of his text, presents an MT data set that includes a tabulation of both apparent resistivity and a standard deviation of uncertainty over a broad range of periods. We'll use this data to provide a benchmark for an order-of-magnitude comparison.

From (3.20) and (3.24) we form the relative error (the standard deviation divided by the mean)

$$R_a \equiv \frac{\sqrt{\delta E\{(\bar{\rho}_a^{hom})^2\}}}{\bar{\rho}_a^{hom}} = \sqrt{\frac{3\delta\gamma^2}{2\bar{\sigma}^2 z_s}}. \quad (3.25)$$

In order to evaluate this expression, we consider a model consisting of layers of thickness \tilde{l} . The conductivities of these layers are assumed to be independent, identically distributed random variables uniformly distributed on the interval $[\sigma_1, \sigma_2]$ (where \tilde{l}, σ_1 and σ_2 represent actual, dimensional values). For this model, R_a reduces to

$$R_a = \left(\frac{\sigma_2 - \sigma_1}{\sigma_2 + \sigma_1} \right) \sqrt{\tilde{l}/(2z_s)}, \quad (3.26)$$

where z_s likewise represents the actual dimensional skin depth for the effective medium half space.

Figure 3 compares R_a with corresponding apparent resistivity quotients formed from Parker's data and plotted as a function of logarithmic frequency. We have used the values $\sigma_2 = 0.1$ S/m, $\sigma_1 = 0.01$ S/m and $\tilde{l} = 3$ m.

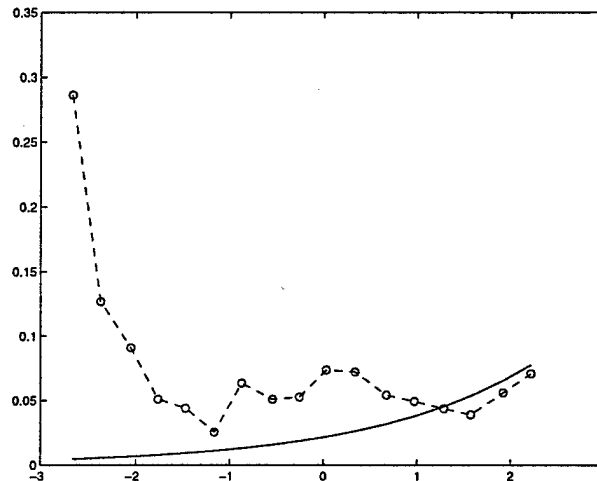


FIGURE 3. Comparison of Uncertainty Levels: Apparent Resistivity Uncertainty *vs.* Logarithm of Frequency (Hz). The solid curve represents uncertainty due to resistivity microstructure. The circles are uncertainty levels reported by Parker [12].

The sources of uncertainty that we compare in Figure 3 are certainly different. However, this graphical comparison does illustrate the fact that a reasonable level of conductivity fluctuations can give rise to uncertainties that are roughly comparable in size over a significant frequency band to those encountered in practice.

4. FUNDAMENTAL LIMITS TO DETECTABILITY

In the interpretation of magnetotelluric surveys it is often assumed that the Earth consists of a discrete number of plane layers, within each of which the conductivity σ is a constant. This type of model ignores small spatial scale random variations, which are always present. In this section we investigate the effect of scattering noise due to the microstructure on the ability of such a survey to detect a particular layer of interest. Since scattering noise is created by the same physical

mechanism as the “signal” from the macroscopic layers, this type of noise represents a fundamental limit to detectability that cannot be reduced by instrumentation.

For a more general plane-layered model that includes the microstructure, we consider σ to be a piecewise-homogeneous random function. We consider m macroscopic layers, with layer boundaries $-L = \bar{z}_m < \bar{z}_{m-1} < \bar{z}_{m-2} < \dots < \bar{z}_0 = 0$. For $\bar{z}_j < z < \bar{z}_{j-1}$, $\sigma = \sigma_j(z/\delta)$, where σ_j is a stationary random process with mean $\bar{\sigma}_j$ and noise strength γ_j^2 . Formulas for rapid calculation of the effective medium impedances and of the covariances for models of this type are derived in Appendix A.

For simplicity, we consider in detail the case $m = 3$, illustrated by Figure 4. The top layer, $\bar{z}_1 < z < \bar{z}_0$ has an average conductivity $\bar{\sigma}_1$ and an effective scattering strength γ_1^2 . These same values are assumed to be taken by the third layer, which lies directly above the basement. Sandwiched between these two layers, in $\bar{z}_2 < z < \bar{z}_1$, is a layer with different values, $\bar{\sigma}_2, \gamma_2^2$.

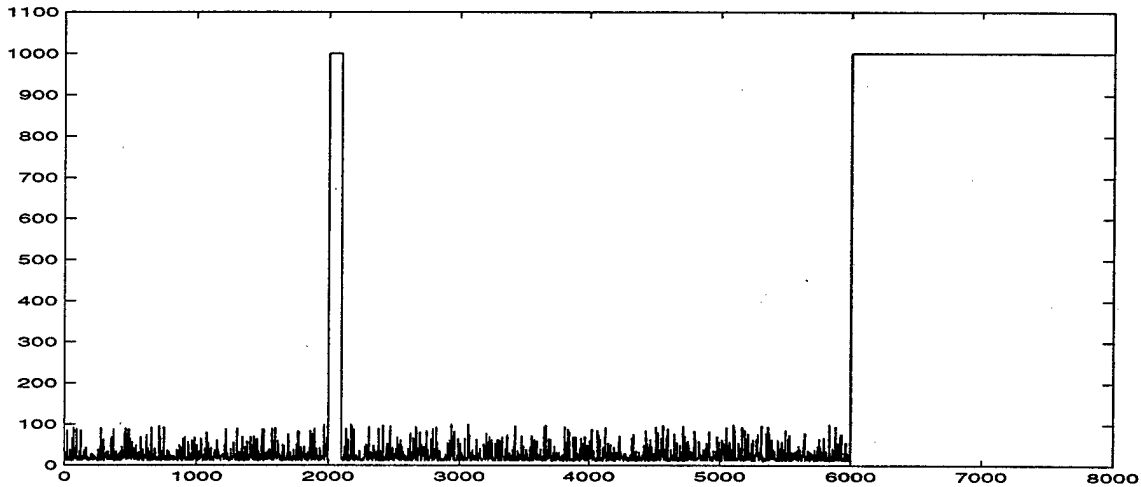


FIGURE 4. Random Three-Layer Model: Resistivity (Ohm-m) vs. Depth (m). A 1000 Ohm-m layer (100 m thick) lies between two layers having randomly-fluctuating microstructure. The semi-infinite basement has a 1000 Ohm-m resistivity.

We investigate here the statistical reliability with which the middle layer can be detected with an MT survey. The existence of this layer, *i.e.* the model shown in Figure 4, is referred to as hypothesis H_1 . This hypothesis is to be contrasted with the one in which the middle layer is not present, *i.e.* there is just one layer, occupying $\bar{z}_3 < z < \bar{z}_0$, with parameters $\bar{\sigma}_1$ and γ_1^2 . This latter hypothesis is referred to as H_0 , the null hypothesis.

This example is a model for MT exploration. Since hot, pressurized brine is highly conducting, $\bar{\sigma}_2 \gg \bar{\sigma}_1$ in prospecting for geothermal energy. Since hydrocarbons are highly resistive, $\bar{\sigma}_2 \ll \bar{\sigma}_1$ in prospecting for oil or gas. In either case, we are to reach a decision H_1 or H_0 , as to whether or not the target has been detected by MT.

Within this framework, there is an optimal method of reaching a decision by processing the survey data. This “most powerful test” is given by the Lemma of Neyman and Pearson [22]. Let the data vector be

$$\mathbf{d} = (\xi_1^R, \xi_2^R, \dots, \xi_N^R, \xi_1^I, \xi_2^I, \dots, \xi_N^I)^T. \quad (4.1)$$

As before, ξ_j^R, ξ_j^I are, respectively, the real and imaginary parts of the impedance at frequencies ω_j measured at the surface $z = 0$.

For $h = 0$ or 1 , let E_h denote the expectation under the assumption of hypothesis H_h . Then, for each case, the mean of the data is

$$\bar{\mathbf{d}}_h = E_h\{\mathbf{d}\} = (\bar{\xi}_{1,h}^R, \bar{\xi}_{2,h}^R, \dots, \bar{\xi}_{N,h}^R, \bar{\xi}_{1,h}^I, \bar{\xi}_{2,h}^I, \dots, \bar{\xi}_{N,h}^I)^T. \quad (4.2)$$

That is, the $2N$ vector of real and imaginary parts of the impedances for the effective medium corresponding to the appropriate hypothesis.

Similarly, putting $\xi_j = \bar{\xi}_j + \sqrt{\delta} \hat{\xi}_j$, the covariance matrix for the data depends upon the hypothesis (H_1 or H_0). For each hypothesis we have

$$\mathbf{C}_h = E_h\{(\mathbf{d} - \bar{\mathbf{d}}_h)(\mathbf{d} - \bar{\mathbf{d}}_h)^T\} = \delta \begin{pmatrix} \mathbf{C}_h^{RR} & \mathbf{C}_h^{RI} \\ \mathbf{C}_h^{IR} & \mathbf{C}_h^{II} \end{pmatrix}. \quad (4.3)$$

That is, the $2N \times 2N$ covariance matrix is partitioned into four $N \times N$ blocks, which can be computed for the appropriate model using the general theory.

Since the data are Gaussian, the probability density of the data vector in $2N$ -dimensional space is, for $h = 0$ or 1 ,

$$P_h(\mathbf{d}) = \frac{\exp[-\frac{1}{2}(\mathbf{d} - \bar{\mathbf{d}}_h)^T \mathbf{C}_h^{-1}(\mathbf{d} - \bar{\mathbf{d}}_h)]}{\sqrt{\det 2\pi \mathbf{C}_h}}. \quad (4.4)$$

The ‘‘most powerful test’’ involves the choice of a threshold $\bar{\theta}$. Given this threshold, we are to decide H_1 whenever

$$\frac{P_1(\mathbf{d})}{P_0(\mathbf{d})} > \bar{\theta}. \quad (4.5)$$

For the Gaussian of (4.4), this test is equivalent to thresholding the quadratic form $Q(\mathbf{d})$, *i.e.*

$$Q(\mathbf{d}) = (\mathbf{d} - \bar{\mathbf{d}}_0)^T \mathbf{C}_0^{-1}(\mathbf{d} - \bar{\mathbf{d}}_0) - (\mathbf{d} - \bar{\mathbf{d}}_1)^T \mathbf{C}_1^{-1}(\mathbf{d} - \bar{\mathbf{d}}_1) > \theta. \quad (4.6)$$

Here, the alternative threshold θ for Q is related to $\bar{\theta}$ by the relation

$$\theta = 2 \log \bar{\theta} + \log \det \mathbf{C}_1 - \log \det \mathbf{C}_0. \quad (4.7)$$

Now, $Q(\mathbf{d})$ has a probability density $q_0(Q)$ if hypothesis H_0 is true and a probability density $q_1(Q)$ if hypothesis H_1 is true. The *false positive rate* P_{FP} is the probability of deciding that a target layer has been detected when, in fact, it is not present. From (4.6)

$$P_{FP} = P_{FP}(\theta) = \int_{\theta}^{\infty} q_0(Q) dQ. \quad (4.8)$$

The *false negative rate*, P_{FN} , is the probability that the decision made will miss a target that is present; so, from (4.6)

$$P_{FN} = P_{FN}(\theta) = \int_{-\infty}^{\theta} q_1(Q) dQ. \quad (4.9)$$

These two types of errors can be traded off against each other by changing the threshold θ . In general, however, one error rate cannot be reduced without increasing the other error rate. The trade-off relation between false positive and false negative error rates is a fundamental limitation on the reliability of detection. It is standard practice in detection theory to illustrate the relation between the error rates by plotting a ROC (Receiver Operating Characteristic) curve, in which the probability of detection, $1 - P_{FN}$, is plotted against the false positive rate, P_{FP} [23]. Since the Neyman-Pearson Lemma guarantees that our data processing is optimal, the ROC curve cannot be

improved. These ideas are illustrated in the next section, where the theory is compared to Monte Carlo simulations.

The above formulas simplify considerably if we make the approximation

$$\mathbf{C}_1 \approx \mathbf{C}_0 \equiv \mathbf{C}. \quad (4.10)$$

This is the case, for instance, when the middle (target) layer is small, and/or the contrast in properties is not great, *i.e.* when detection is difficult. If (4.10) is valid, then the quadratic terms in (4.6) cancel and Q becomes linear, *i.e.*

$$\begin{aligned} Q &\approx 2(\bar{\mathbf{d}}_1 - \bar{\mathbf{d}}_0)^T \mathbf{C}^{-1} \mathbf{d} - \bar{\mathbf{d}}_1^T \mathbf{C}^{-1} \bar{\mathbf{d}}_1 + \bar{\mathbf{d}}_0^T \mathbf{C}^{-1} \bar{\mathbf{d}}_0 \\ &= (\bar{\mathbf{d}}_1 - \bar{\mathbf{d}}_0)^T \mathbf{C}^{-1} (2\mathbf{d} - \bar{\mathbf{d}}_1 - \bar{\mathbf{d}}_0). \end{aligned} \quad (4.11)$$

Under hypotheses H_0 and H_1 , respectively, linearized Q has mean values

$$\begin{aligned} Q_0 &= E_0\{Q\} = -(\bar{\mathbf{d}}_1 - \bar{\mathbf{d}}_0)^T \mathbf{C}^{-1} (\bar{\mathbf{d}}_1 - \bar{\mathbf{d}}_0) \\ Q_1 &= E_1\{Q\} = (\bar{\mathbf{d}}_1 - \bar{\mathbf{d}}_0)^T \mathbf{C}^{-1} (\bar{\mathbf{d}}_1 - \bar{\mathbf{d}}_0). \end{aligned} \quad (4.12)$$

Under either hypothesis, Q has standard deviation S , where

$$S = 2\sqrt{(\bar{\mathbf{d}}_1 - \bar{\mathbf{d}}_0)^T \mathbf{C}^{-1} (\bar{\mathbf{d}}_1 - \bar{\mathbf{d}}_0)} = 2\sqrt{Q_1}. \quad (4.13)$$

Using (4.11) and (4.12), the false positive and false negative error rates for the optimal test (4.6) can be represented using the cumulative normal probability distribution function

$$F(a) = \frac{1}{\sqrt{2\pi}} \int_{-\infty}^a \exp(-\tau^2/2) d\tau. \quad (4.14)$$

Then

$$\begin{aligned} P_{FP} &= P_{FP}(\theta) = 1 - F\left(\frac{\theta - Q_0}{S}\right) \\ P_{FN} &= P_{FN}(\theta) = F\left(\frac{\theta - Q_1}{S}\right). \end{aligned} \quad (4.15)$$

Approximation (4.10) also simplifies the analysis of stacked data. Suppose that data vectors of the form (4.1) are collected from r different locations, widely separated on the surface. If it is assumed that the macrostructure is identical at each location, but that the microstructures are statistically independent (with identical probabilities), then the data vectors may be considered to be r independent, identically distributed samples. The optimal test then utilizes only the average of the r vectors; this average is used in place of \mathbf{d} in equation (4.11). The resulting Q is then compared to a threshold. Stacking reduces the errors; the stacked error rates become

$$\begin{aligned} P_{FP}^{stack}(\theta) &= 1 - F\left(\frac{(\theta - Q_0)\sqrt{r}}{S}\right) \\ P_{FN}^{stack}(\theta) &= F\left(\frac{(\theta - Q_1)\sqrt{r}}{S}\right) \end{aligned} \quad (4.16)$$

5. MONTE CARLO SIMULATIONS

We use the three-layer model shown in Figure 4 as a prototype to numerically study and evaluate the theory. A semi-infinite basement having a constant 1000 Ohm-m resistivity is assumed to occupy the region $z \leq -6000$ m. A thin, highly resistive layer of interest (100 m thick with 1000 Ohm-m resistivity) is positioned at a depth of 2000 m, *i.e.* $-2100 \text{ m} \leq z \leq -2000 \text{ m}$. The intervening regions, $-6000 \text{ m} \leq z \leq -2100 \text{ m}$ and $-2000 \text{ m} \leq z \leq 0 \text{ m}$ consist of random layers having independent, identically distributed conductivities. Since MT is quite insensitive to resistive targets in conductive backgrounds, this is a good test. Recall that the theory possesses a robustness with respect to microstructure details; it predicts that the statistical behavior of the impedance and apparent resistivity depends only upon the mean conductivity $\bar{\sigma}(z)$ and the fluctuation parameter $\delta\gamma^2$ and not upon the details of the statistical model generating these parameters. To provide some illustration of this robustness, we consider two statistical models. In the first model, the layer conductivities are uniformly distributed on the interval $0.01 \text{ S/m} \leq \sigma \leq 0.10 \text{ S/m}$ and the layers are each assumed to be a constant 3 m in thickness. In the second model, the layer thicknesses are also randomized with a uniform distribution on the interval $1 \text{ m} \leq l \leq 5 \text{ m}$. The layer conductivities are again assumed to be independent and identically, uniformly distributed. In this case, since the mean layer thickness is again 3 m, one can show that the conductivity interval generating the same values of $\bar{\sigma}$ and $\delta\gamma^2$ remains the same.

Two cases, where the thin resistive layer is both present and absent, are considered. (When the thin layer is absent, the random layering is simply taken to occupy the entire interval $-6000 \text{ m} \leq z \leq 0 \text{ m}$.) 5000 realizations were generated for each case (*i.e.* thin layer present and absent) and for each random layering model. Fifty one frequencies, equally spaced on a logarithmic scale extending from -2 to 3 , were considered. The results are displayed in Figure 5. We plot the apparent resistivity mean and the mean \pm one standard deviation over the frequency range $10^{-2} \leq f \leq 10^3$. Simulation results for the two random models are compared with the theoretical predictions. Agreement is good over the entire five decade frequency band. As one would expect, the resistivity fluctuations decrease as frequency decreases. Moreover, as frequency decreases, the entire 6 kilometers of random layering (with the thin resistive target layer present or not) becomes increasingly transparent and the surface apparent resistivity tends toward the 1000 Ohm-m value of the semi-infinite basement.

Figures 6 offer additional evidence of good agreement between the theory and simulations for the real and imaginary parts of the impedance and for the apparent resistivity. The first two plots compare predicted (Gaussian) and computed probability density functions for the real and imaginary parts of the impedance, respectively, at 1 Hz. Note that for both impedance components the variance is small, on the order of 10^{-4} , so that the peak density value is correspondingly on the order of thousands. The imaginary part is negative and roughly equal in magnitude to its real counterpart, as one would expect (*i.e.* the impedance phase is roughly -45°). The third of Figures 6 presents an analogous comparison of theory and simulations for the apparent resistivity at 1 Hz. (For simplicity, the simulations used in these and all subsequent plots are those involving the fixed 3 m layer thickness.)

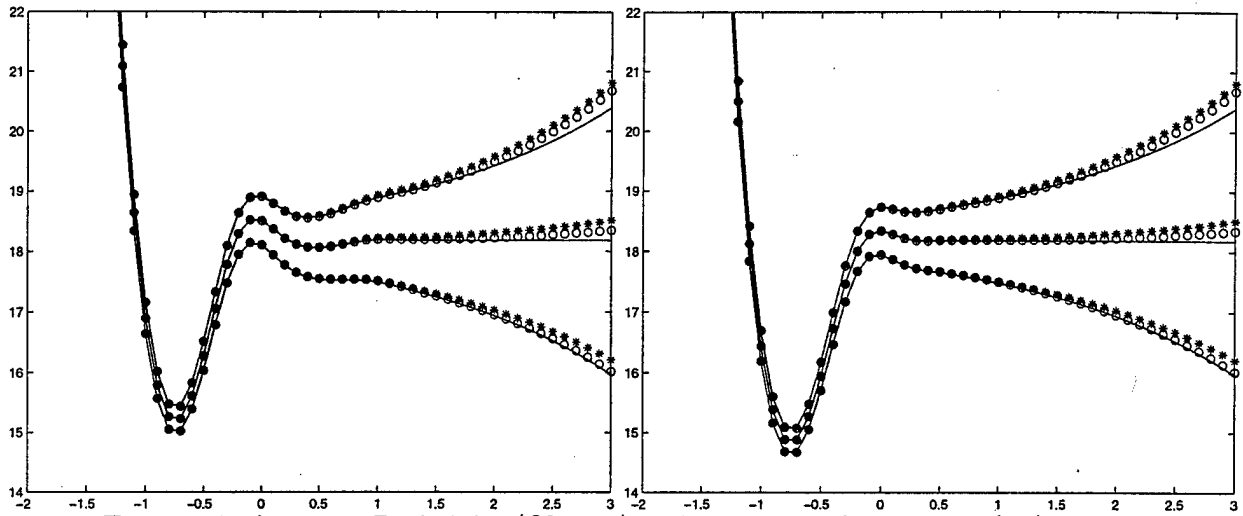


FIGURE 5. Apparent Resistivity (Ohm-m) *vs.* Logarithm of Frequency (Hz): a comparison of theory and simulations. The mean and mean \pm one standard deviation are plotted for (a) the thin resistive layer present and (b) the layer absent. The solid lines represent the theory. The circles and stars represent the two random layering models used in the simulations.

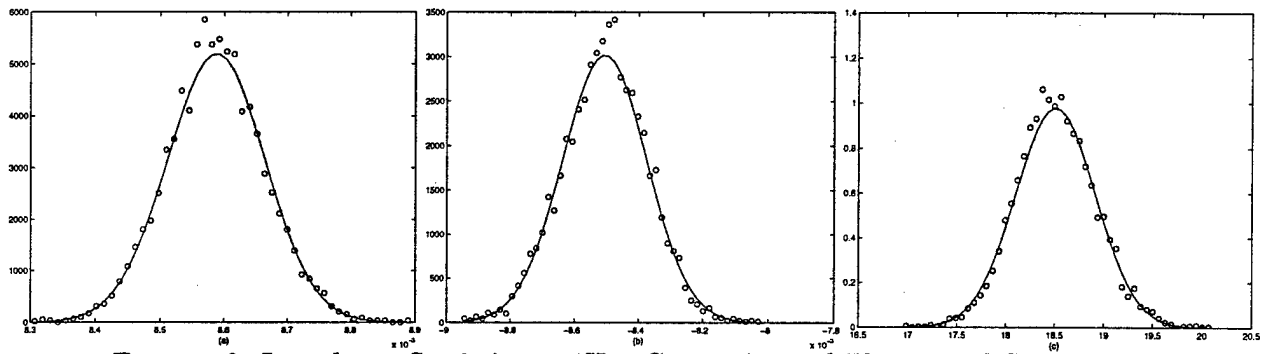


FIGURE 6. Impedance Statistics at 1Hz: Comparison of Theory and Simulations. Probability density functions predicted by the theory (solid curves) and constructed from the simulations (circles) are shown for (a) the real part of the impedance, (b) the imaginary part of the impedance and (c) the apparent resistivity.

Since the number of frequencies $N = 51$ in our calculations, covariance matrices C_h , $h = 0, 1$, as given by (4.3), are 102×102 real symmetric arrays. In Figures 7 we display surface plots of the covariance matrix subblocks C_1^{RR} , C_1^{II} and C_1^{RI} as functions of logarithmic frequency. Although the particular case shown corresponds to that computed from the simulations with the thin, highly resistive layer present, the other possibilities (theory *vs.* simulations, layer present *vs.* layer absent) all produce indistinguishable results on the scale shown. The behavior shown is what one would expect. As frequency increases, random fluctuations in both the real and imaginary parts of the impedance increase in amplitude. Therefore, as one moves out along the main diagonal in the first and third plots, the corresponding variances likewise increase; variances of the imaginary part are larger than their real counterparts. As the second of Figures 7 shows, the real-imaginary cross-correlations are likewise largest in amplitude at the highest frequencies. Note that the behavior

of the fluctuations is coupled so that this fluctuation product is negative. (This negative value agrees with analogous cross-correlation results obtained for the homogeneous random half space; *c.f.* (3.13), (3.14).)

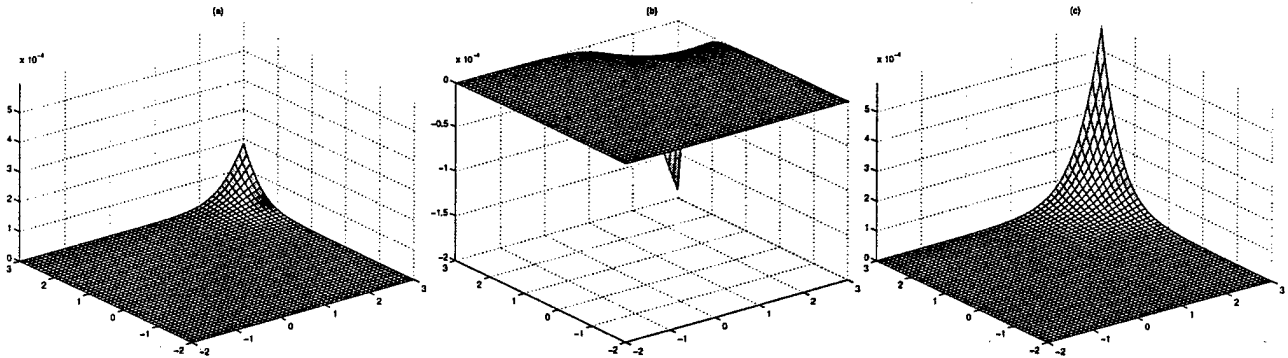


FIGURE 7. Covariance Submatrices: (a) Real-Real C^{RR} , (b) Real-Imaginary C^{RI} , and (c) Imaginary-Imaginary C^{II} Covariance Submatrices are plotted against Logarithm of Frequency.

Figures 7 suggest a large spread in the amplitudes of the covariance matrix elements but mask the low frequency fine structure. Such a large range of amplitudes is not surprising, given the results of Section 3 for the homogeneous random half space. Note in particular the frequency dependence in (3.13) and (3.14), together with the fact that the frequency range considered spans five decades. The matrix elements in Figures 7 have amplitudes ranging roughly from 6×10^{-4} to 6×10^{-11} .

Figures 8 study the real-real covariance subblock C^{RR} as a representative case; results for the other subblocks are qualitatively similar. The first two plots display the low frequency structure for theory and simulations, respectively. The third and fourth plots, on the other hand, study the impact of the thin resistive layer upon this covariance subblock; $C_1^{RR} - C_0^{RR}$ is plotted for both theory and simulations. These plots further confirm the good agreement between theory and simulations. They also lend credence to approximation (4.10)

Low frequency surface impedance information is very important in detecting the presence or absence of a thin, highly resistive layer such as that shown in Figure 4. Higher frequencies correspond to both shorter skin depths and increased impedance fluctuation levels due to the random conductivity microstructure. At low frequencies, sources of noise other than conductivity microstructure assume increasing importance; this is certainly suggested by the Parker data [12] in Figure 3.

We will model other sources of noise with an additional white noise component. That is, the measured impedance will be taken to be

$$\xi_j^R + \nu_j^R + i(\xi_j^I + \nu_j^I), \quad j = 1, \dots, N, \quad (5.1)$$

where $\{\nu_j^R, \nu_j^I\}_{j=1}^N$ is a family of independent, identically-distributed, zero mean Gaussian random variables having common (dimensional) variance ν^2 . As a result of this modification, the mean or effective impedances $\bar{\xi}_j$ remain unchanged but the covariance matrix undergoes the change $\delta C \rightarrow \delta C + \nu^2 I$.

The detection problem can be summarized by examining Figure 9. Assuming $\nu^2 = 10^{-9}$, we have plotted the mean apparent resistivity and the mean \pm one standard deviation for each of the

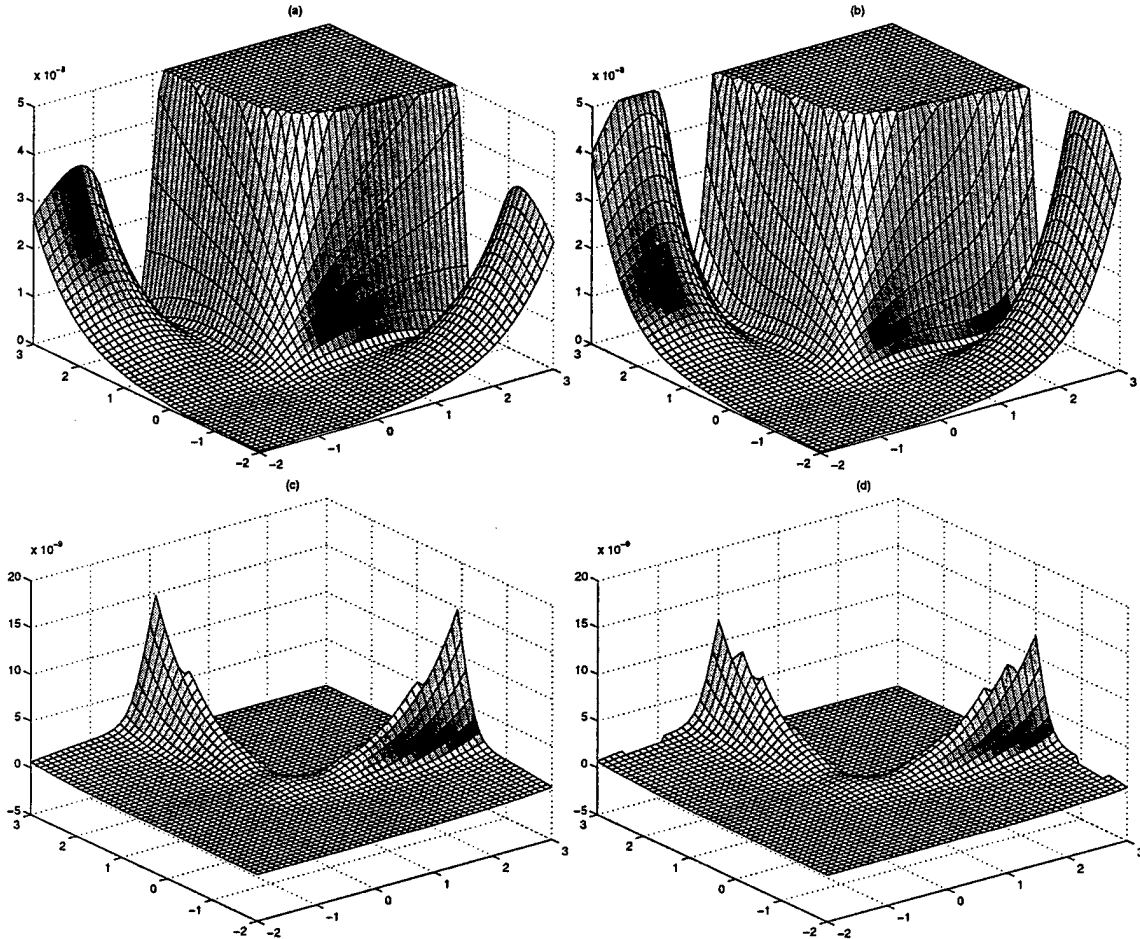


FIGURE 8. Real-Real Covariance Submatrix *vs.* Logarithmic Frequency. The first two figures show the fine scale structure of C^{RR} , as computed by (a) theory and (b) simulations. The latter two figures show the effect of the thin resistive layer upon the covariance submatrix, *i.e.* $C_1^{RR} - C_0^{RR}$, as computed by theory in (c) and simulations in (d).

two cases; the solid-line curves represent the case where the thin resistive layer is present (H_1 true) while the dashed curves correspond to the layer being absent (H_0 true). The circles and stars, on the other hand, represent two sets of measurements, in this case two simulation realizations, both with the layer present. Given just one of these sets of measurements, we must decide whether or not the layer is present.

We attack this detection problem using the ideas of Section 4. In order to determine the false positive and false negative rates associated with this problem, *i.e.* P_{FP} and P_{FN} as given by (4.8), (4.9), we must determine the probability density functions q_0 and q_1 present in the integrands. We have numerically determined these density functions for the quadratic functional $Q(d)$ in (4.6) and found that the approximation $C_0 \approx C_1$, leading to (4.11), is a very good one for our model problem. As noted in Section 4, this linearizing approximation reduces $Q(d)$ to a Gaussian random variable with known mean and variance and makes the theory very easy to implement. Ultimately, we eliminate the threshold parameter to obtain P_{FP} *vs.* P_{FN} . This relation is plotted as a ROC curve, *i.e.* the detection probability, $1 - P_{FN}$, is plotted against the false positive rate, P_{FP} .

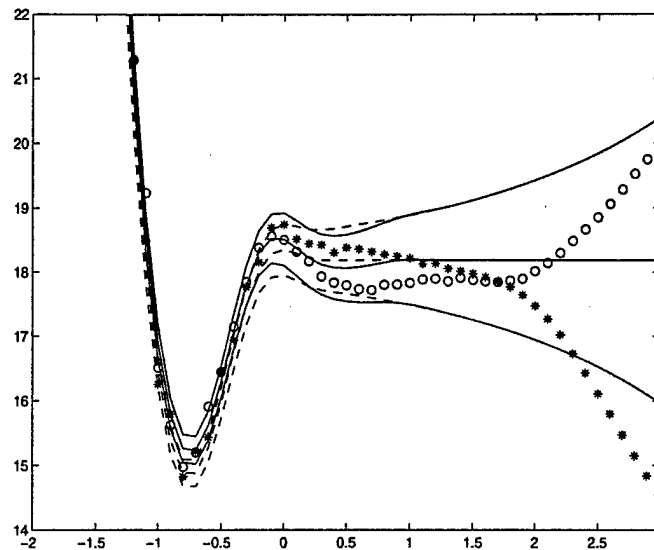


FIGURE 9. The Detection Problem: Apparent Resistivity (Ohm-m) *vs.* Logarithm of Frequency (Hz). The solid and dashed curves are predictions of the theory for the resistive layer being present and absent, respectively. The mean and mean \pm one standard deviation are shown for each case. The circles and stars are two different realizations, *i.e.* two different sets of random microstructure, both for the case where the layer is present.

To illustrate these ideas, consider a case where an added white noise level $\nu^2 = 10^{-9}$ exists and the highly resistive layer, with its upper surface remaining at a depth of 2000 m, has its thickness reduced from an initial 100 m to a final 10 m. We expect the layer detection to become increasingly difficult as its thickness is reduced. Figures 10 illustrate these ideas at the level of the probability density functions $q_h(Q)$. The two plots correspond to layer thicknesses of 100 m and 25 m, respectively. In the first case, the density functions q_1 and q_0 , (corresponding to the 100 m layer being present and absent), are quite separated. Given a single realization, *i.e.* a single set of surface impedance measurements, one could therefore, with relatively high probability, correctly decide upon the presence or absence of the resistive layer. (If the density functions had completely disjoint supports, a single realization would with certainty answer the detection question.) As the layer thickness decreases, the density functions tend to peak and migrate toward each other; for the 25 m thick layer shown in the second plot, the two density functions have considerable overlap. In this case, given a single realization, identifying the correct hypothesis is correspondingly more difficult. In the extreme case where both density functions completely overlap, the realization (*i.e.* the set of impedance measurements) would provide no useful detection information.

Symmetries are evident in Figures 10. The density functions q_0 and q_1 are Gaussian with equal variances and means symmetrically located relative to the origin. This structure follows from (4.11)-(4.13).

Recall that Figure 9 includes apparent resistivity plots for two realizations (*i.e.* different random microstructures), both with the 100 m resistive layer present. One can ask, in the context of the optimal detection theory presented, "How detectable is the resistive layer in each of these two particular cases?". The quadratic form $Q(\mathbf{d})$ defined by (4.6) has values of 17.7 and -2.1 for the

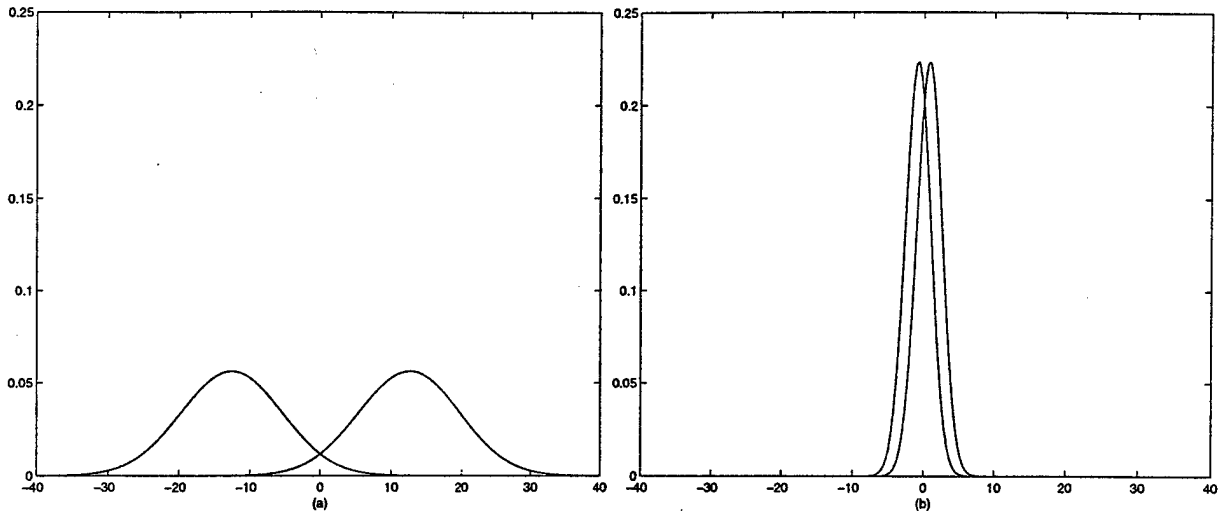


FIGURE 10. Probability Density Functions for the Detection Problem: Density functions q_0 and q_1 for a (a) 100 m thick resistive layer and (b) 25 m layer. In each case, the density function $q_0(Q)$, corresponding to the layer absent, appears on the left while the density function $q_1(Q)$, corresponding to the layer present, appears on the right.

“circles” and “stars” data, respectively. Locating these abscissa values on the first of Figures 10 shows that the 17.7 value is well within the probability mass of q_1 , essentially disjoint from the the probability mass of q_0 , while the -2.1 value is in the overlap region of the q_0 and q_1 density tails. In the former case, detection of the resistive layer would be relatively straightforward. Noting (4.9), $\theta = 17.7$ corresponds to $P_{FN} = 0.78$; any false negative threshold less than this value would result in the correct detection of the layer. On the other hand, $\theta = -2.1$ corresponds to $P_{FN} = 0.01$ and any higher threshold would cause the layer to be missed.

In Figures 11, the performance of the optimal detector is illustrated by its ROC curve: that is, the probability of detection, $1 - P_{FN}$, is plotted against the false positive rate P_{FP} . When the two probability densities q_0 and q_1 are well separated, good detection is possible. In this case the probability of detection is close to one unless the false positive rate is kept very small. Therefore the ROC curve, which always passes through the origin, rises steeply to unity in this case. At the other extreme, when the two probability densities q_0 and q_1 substantially overlap, detection will be poor. In this case the ROC curve lies close to the diagonal line where the detection probability equals the false positive rate; hence the detector performs no better than the flip of a biased coin. Figures 11 clearly show a progression from one extreme to the other as the resistive layer thickness is reduced from 100 m to 10 m.

One can similarly study the detection question as other parameters are varied, *e.g.* one where resistive layer thickness is held fixed but the level of additive noise is varied. Figure 12 shows what happens, for the case of the 50 m layer, as the level of additive noise is increased from $\nu^2 = 10^{-11}$ to $\nu^2 = 10^{-5}$. At the lowest 10^{-11} noise level, the ROC curve predicts almost certain detection, unless the false positive rate is kept very low. At the highest 10^{-5} noise level, the detection curve is basically the straight line of equal probabilities. In this case the added noise has corrupted the measurements to the point that they no longer provide useful detection information.

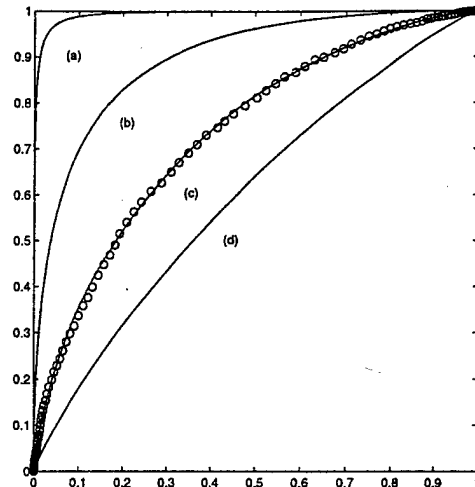


FIGURE 11. ROC Curves: Probability of Detection *vs.* False Positive Rate for a resistive layer thickness of (a) 100 m, (b) 50 m, (c) 25 m, (d) 10 m, constructed using the theory. The circles represent a corresponding curve created using the simulations.

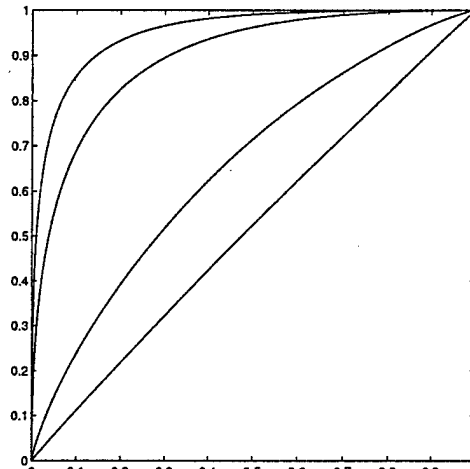


FIGURE 12. The Effect of Added Noise upon Detection: ROC curves are plotted for a resistive layer thickness of 50 m and added noise levels of $\nu^2 = 10^{-11}, 10^{-9}, 10^{-7},$ and 10^{-5} . The curves decrease monotonically as the noise level is increased.

A final point worth emphasizing is the important role that the correct covariance matrices play in the detection process. Figure 13 illustrates this for the case of a 50 m thick resistive layer and an additive noise level of $\nu^2 = 10^{-11}$. The solid curve is the ROC curve computed using the correct covariance matrix. The dashed curve, on the other hand, represents the performance of a detector which assumes that the covariance matrix is the identity matrix. (Any multiple of the identity matrix would correspondingly change the threshold level but not change the resulting ROC curve.) The improvement in detection capability achieved by using the correct covariance matrix is pronounced.

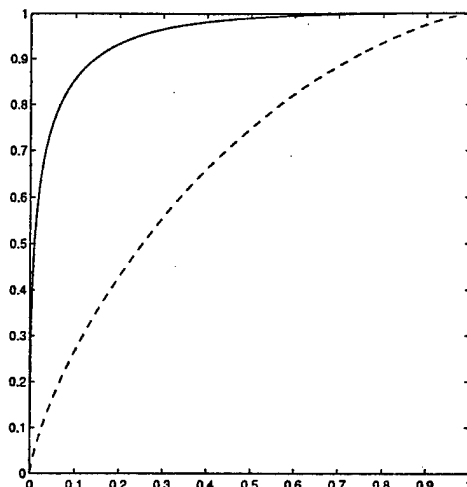


FIGURE 13. The Importance of Using Correct Covariance Information: the case of detecting a 50 m thick resistive layer in the presence of $\nu^2 = 10^{-11}$ added noise is considered. The solid curve is the ROC curve using correct covariance information while the dashed curve represents the case where these covariance weights have been replaced by the identity matrix.

6. CONCLUSIONS

The Monte Carlo simulations verify the accuracy of both the effective medium theory and the theory of random scattering statistics over a frequency range spanning five orders of magnitude. Although the scattering noise is significant compared with estimates of other noise sources, its effects can be substantially mitigated, in the models considered here, using the theory of this paper. If other sources of noise can be sufficiently reduced, good detection is possible, in these models, for relatively thin layers of anomalous resistivity at depth. However, good detection levels are achieved only through use of optimal detection algorithms, which incorporate a theoretical understanding of the noise statistics.

REFERENCES

- [1] Vozoff, K., The magnetotelluric method, 1991, *Electromagnetic Methods in Applied Geophysics - Applications*, Chapter 8, edited by Nabighian, M. N., Society of Exploration Geophysicists.
- [2] Zhdanov, M. S. and Keller, G. V., 1994, *The Geoelectrical Methods in Geophysical Exploration*, Elsevier.
- [3] Berdichevsky, M. N. and Zhdanov, M. S., 1984, *Advanced Theory of Deep Geomagnetic Sounding*, Elsevier.
- [4] Courant, R. and Hilbert, D., 1962, *Methods of Mathematical Physics*, vol. II, Ch. III, John Wiley and Sons.
- [5] Tikhonov, A. N. 1943, The stability of inverse problems, *Dokl. Akad. Nauk. SSSR*, **39**, 195-198.
- [6] Tikhonov, A. N., 1950, On determination of electrical characteristics of deep layers of the Earth's crust, *Dokl. Akad. Nauk. SSSR*, **73**, 295-297.
- [7] Tikhonov, A. N., 1963, On solution of ill-posed problems and method of regularization, *Dokl. Akad. Nauk. SSSR*, **151**, 501-504.
- [8] Tikhonov, A. N., 1963, On regularization of ill-posed problems, *Dokl. Akad. Nauk. SSSR*, **153**, 49-52.
- [9] Cagniard, L., 1953, Basic theory of the magneto-telluric method of geophysical prospecting, *Geophysics*, **18**, 605-635.
- [10] Weidelt, P., 1972, The Inverse Problem of Geomagnetic Induction, *Zeitschrift fur Geophysik*, **38**, 257-289.
- [11] Tikhonov, A. N. and Arsenin, V. Y., 1977, *Solutions of Ill-Posed Problems*, V. H. Winston and Sons.
- [12] Parker, R. L., 1994, *Geophysical Inverse Theory*, Princeton University Press.
- [13] O'Doherty, R. F., and Anstey, N. A., 1971, Reflections on amplitudes, *Geophys. Prosp.*, **19**, 430-458.
- [14] Godfrey, R., Muir, F., and Rocca, F., 1980, Modeling seismic impedance with Markov chains, *Geophysics*, **45**: 1351-1372.
- [15] Banik, N. C., Lerche, I., Resnick, J. R., and Shuey, R. T., 1985, Stratigraphic filtering, Part II: Model spectra: *Geophysics*, **50**, 2775-2783.
- [16] White, B., Sheng, P. and Nair, B., 1990, Localization and backscattering spectrum of seismic waves in stratified lithology, *Geophysics*, **55**, 1158-1165.
- [17] Walden, A. T., and Hosken, J. W. J., 1985, An investigation of the spectral properties of primary reflection coefficients, *Geophys. Prosp.*, **33**, 400-435.
- [18] Velzeboer, C. J., 1981, The theoretical seismic reflection response of sedimentary sequences, *Geophysics*, **46**, 843-853.
- [19] Sato, H., 1984, Attenuation and Envelope Formation of Three-Component Seismograms of Small Local Earthquakes in Randomly Inhomogeneous Lithosphere, *Journal of Geophysical Research*, **89**, B2, 1221-1241.
- [20] Asch, M., Kohler, W., Papanicolaou, G., Postel, M., and White, B., 1991, Frequency content of randomly scattered signals, *SIAM Review*, **33**, 519-625.
- [21] Khasminskii, R. Z., 1966, On stochastic processes defined by differential equations with a small parameter, *Theory of Probability and its Applications*, **11**, 211-228.
- [22] Gnedenko, B. V., 1962, *The Theory of Probability*, Chelsea Publishing Company.
- [23] Melsa, J. A. and Cohn, D. L., 1978, *Decision and Estimation Theory*, McGraw-Hill.
- [24] Tarantola, A., 1987, *Inverse Problem Theory*, Elsevier.
- [25] Oksendal, B., 1985, *Stochastic Differential Equations*, Springer-Verlag.

APPENDIX A. PIECEWISE-HOMOGENEOUS RANDOM MEDIA

In this appendix we consider piecewise-homogeneous random media of the type introduced in Section 4. These types of models generalize the usual macroscopic layer models to include the effects of random scattering from the microstructure.

Consider m macroscopic layers, with layer boundaries $-L = \bar{z}_m < \bar{z}_{m-1} < \bar{z}_{m-2} < \dots < \bar{z}_0 = 0$. For $\bar{z}_r < z < \bar{z}_{r-1}$, $\sigma = \sigma_r(z/\delta)$, where σ_r is a stationary random process with mean $\bar{\sigma}_r$ and noise strength γ_r^2 . Consider the interface at $z = \bar{z}_r$ for some r . We assume that $\bar{\xi}(\bar{z}_r)$, $\hat{C}(\bar{z}_r)$ and $\bar{C}(\bar{z}_r)$ have been determined. (Recall that $\bar{\xi}$, \hat{C} and \bar{C} are all continuous across the interface.) We will next derive formulas for $\bar{\xi}(z)$, $\hat{C}(z)$ and $\bar{C}(z)$ for $z_r < z < z_{r-1}$. Using these formulas recursively, one can compute the relevant quantities at $z = 0$ rapidly, by stepping up from the basement layer-by-layer. We write $\bar{\sigma} = \bar{\sigma}_r$, $\gamma = \gamma_r$ and $\bar{z} = \bar{z}_r$. Let

$$V_j = \exp\left(\bar{\sigma} \int_{\bar{z}_0}^z \bar{\xi}_j(s) ds\right), \quad (\text{A.1})$$

where the j -subscript refers to frequency ω_j . Then

$$\frac{d}{dz} V_j = \bar{\sigma} \bar{\xi}_j V_j \quad (\text{A.2})$$

and

$$\frac{d^2}{dz^2} V_j + k_j^2 V_j = 0, \quad (\text{A.3})$$

where

$$k_j = \sqrt{\omega_j \mu \bar{\sigma}} e^{i\pi/4}. \quad (\text{A.4})$$

Since from (A.1), (A.2)

$$\begin{aligned} V_j(\bar{z}) &= 1 \\ \frac{d}{dz} V_j(\bar{z}) &= \bar{\sigma} \bar{\xi}_{0,j}, \end{aligned} \quad (\text{A.5})$$

we obtain from (A.3), (A.5) that

$$V_j = A_j \exp[ik_j(z - \bar{z})] + B_j \exp[-ik_j(z - \bar{z})], \quad (\text{A.6})$$

where

$$\begin{aligned} A_j &= \frac{1}{2} \left(1 + \frac{\bar{\sigma} \bar{\xi}_{0,j}}{ik_j}\right) \\ B_j &= \frac{1}{2} \left(1 - \frac{\bar{\sigma} \bar{\xi}_{0,j}}{ik_j}\right). \end{aligned} \quad (\text{A.7})$$

Solving (A.2) for $\bar{\xi}_j$ and substituting from (A.6) yields

$$\bar{\xi}_j = \frac{ik_j}{\bar{\sigma}} \left(\frac{A_j \exp[ik_j(z - \bar{z})] - B_j \exp[-ik_j(z - \bar{z})]}{A_j \exp[ik_j(z - \bar{z})] + B_j \exp[-ik_j(z - \bar{z})]} \right). \quad (\text{A.8})$$

From (A.8) $\bar{\xi}_j$ can be determined at the next layer boundary, $z = \bar{z}_{r-1}$. Formula (A.8) is well known in the literature [2].

Next, $V_j^2 V_l^2$ may be identified as an integrating factor in equation (3.7), *i.e.*

$$\frac{d}{dz} \left(V_j^2 V_l^2 \hat{C}_{jl} \right) = \gamma^2 V_j^2 V_l^2 \bar{\xi}_j^2 \bar{\xi}_l^2. \quad (\text{A.9})$$

However, from (A.2), (A.6) we obtain

$$V_j \bar{\xi}_j = \frac{ik_j}{\bar{\sigma}} (A_j \exp[ik_j(z - \bar{z})] - B_j \exp[-ik_j(z - \bar{z})]). \quad (\text{A.10})$$

Now, substitution of (A.10) into (A.9) yields

$$\hat{C}_{jl}(z) = \frac{1}{V_j^2(z)V_l^2(z)} \left(\hat{C}_{jl}(\bar{z}) + \gamma^2 \int_{\bar{z}}^z V_j^2 V_l^2 \bar{\xi}_j^2 \bar{\xi}_l^2 ds \right), \quad (\text{A.11})$$

where the integral is

$$\begin{aligned} \int_{\bar{z}}^z V_j^2 V_l^2 \bar{\xi}_j^2 \bar{\xi}_l^2 ds &= \left(\frac{k_j k_l}{\bar{\sigma}^2} \right)^2 \left(A_j^2 A_l^2 \frac{(\exp[2i(k_j + k_l)(z - \bar{z})] - 1)}{2i(k_j + k_l)} \right. \\ &+ A_j^2 B_l^2 \frac{(\exp[2i(k_j - k_l)(z - \bar{z})] - 1)}{2i(k_j - k_l)} - 2A_j^2 A_l B_l \frac{(\exp[2ik_j(z - \bar{z})] - 1)}{2ik_j} \\ &+ B_j^2 A_l^2 \frac{(\exp[2i(k_l - k_j)(z - \bar{z})] - 1)}{2i(k_l - k_j)} + B_j^2 B_l^2 \frac{(\exp[-2i(k_j + k_l)(z - \bar{z})] - 1)}{-2i(k_j + k_l)} \\ &- 2B_j^2 A_l B_l \frac{(\exp[-2ik_j(z - \bar{z})] - 1)}{-2ik_j} - 2A_j B_j A_l^2 \frac{(\exp[2ik_l(z - \bar{z})] - 1)}{2ik_l} \\ &\left. - 2A_j B_j B_l^2 \frac{(\exp[-2ik_l(z - \bar{z})] - 1)}{-2ik_l} + 4A_j B_j A_l B_l (z - \bar{z}) \right). \end{aligned} \quad (\text{A.12})$$

When $j = l$ in (A.12), indeterminate quotients, such as $(\exp[2i(k_j - k_l)(z - \bar{z})] - 1)/2i(k_j - k_l)$, must be replaced by the limiting value $(z - \bar{z})$.

Similarly, $V_j^2(V_l^*)^2$ is an integrating factor in (3.9). We obtain

$$\bar{C}_{jl}(z) = \frac{1}{V_j^2(z)(V_l^*)^2(z)} \left(\bar{C}_{jl}(\bar{z}) + \gamma^2 \int_{\bar{z}}^z (V_j \bar{\xi}_j)^2 (V_l^* \bar{\xi}_l^*)^2 ds \right), \quad (\text{A.13})$$

where the integral can be evaluated to be

$$\begin{aligned} \int_{\bar{z}}^z (V_j \bar{\xi}_j)^2 (V_l^* \bar{\xi}_l^*)^2 ds &= \left(\frac{k_j k_l^*}{\bar{\sigma}^2} \right)^2 \left(A_j^2 (A_l^*)^2 \frac{(\exp[2i(k_j - k_l^*)(z - \bar{z})] - 1)}{2i(k_j - k_l^*)} \right. \\ &+ A_j^2 (B_l^*)^2 \frac{(\exp[2i(k_j + k_l^*)(z - \bar{z})] - 1)}{2i(k_j + k_l^*)} - 2A_j^2 A_l^* B_l^* \frac{(\exp[2ik_j(z - \bar{z})] - 1)}{2ik_j} \\ &+ B_j^2 (A_l^*)^2 \frac{(\exp[-2i(k_j + k_l^*)(z - \bar{z})] - 1)}{-2i(k_j + k_l^*)} + B_j^2 (B_l^*)^2 \frac{(\exp[2i(k_l^* - k_j)(z - \bar{z})] - 1)}{2i(k_l^* - k_j)} \\ &- 2B_j^2 A_l^* B_l^* \frac{(\exp[-2ik_j(z - \bar{z})] - 1)}{-2ik_j} - 2A_j B_j (A_l^*)^2 \frac{(\exp[-2ik_l^*(z - \bar{z})] - 1)}{-2ik_l^*} \\ &\left. - 2A_j B_j (B_l^*)^2 \frac{(\exp[2ik_l^*(z - \bar{z})] - 1)}{2ik_l^*} + 4A_j B_j A_l^* B_l^* (z - \bar{z}) \right). \end{aligned} \quad (\text{A.14})$$

BENJAMIN WHITE, EXXON RESEARCH AND ENGINEERING COMPANY, ROUTE 22E, ANNANDALE, NJ 08801

WERNER KOHLER, DEPARTMENT OF MATHEMATICS, VIRGINIA TECH, BLACKSBURG, VA 24061

LEONARD J. SRNKA, EXXON EXPLORATION COMPANY, P. O. BOX 4778, HOUSTON, TX 77210